Monthly Notices
of the
ROYAL ASTRONOMICAL SOCIETY

MNRAS **458,** 84–104 (2016) doi:10.1093/mnras/stw063

A *Hubble Space Telescope* survey of the host galaxies of Superluminous Supernovae

C. R. Angus,[1⋆] A. J. Levan,[1] D. A. Perley,[2,3] N. R. Tanvir,[4] J. D. Lyman,[1] E. R. Stanway[1] and A. S. Fruchter[5]

[1]*Department of Physics, University of Warwick, Coventry CV4 7AL, UK*
[2]*Dark Cosmology Centre, Niels Bohr Institute, University of Copenhagen, Juliane Maries Vej 30, DK-2100 Copenhagen, Denmark*
[3]*Department of Astronomy, California Institute of Technology, Pasadena, CA 91106, USA*
[4]*Department of Physics and Astronomy, University of Leicester, Leicester LE1 7RH, UK*
[5]*Space Telescope Science Institute, 3700 San Martin Drive, Baltimore, MD 21218, USA*

Accepted 2016 January 7. Received 2016 January 7; in original form 2015 September 4

ABSTRACT

We present *Hubble Space Telescope* (*HST*) Wide Field Camera 3 UV and near-IR (nIR) imaging of 21 Superluminous Supernovae (SLSNe) host galaxies, providing a sensitive probe of star formation and stellar mass within the hosts. Comparing the photometric and morphological properties of these host galaxies with those of core-collapse supernovae (CCSNe) and long-duration gamma-ray bursts (LGRBs), we find SLSN hosts are fainter and more compact at both UV and nIR wavelengths, in some cases we barely recover hosts with absolute magnitude around $M_V \approx -14$. With the addition of ground based optical observations and archival results, we produce spectral energy distribution fits to these hosts, and show that SLSN hosts possess lower stellar mass and star formation rates. This is most pronounced for the hydrogen deficient Type-I SLSN hosts, although Type-II H-rich SLSN host galaxies remain distinct from the bulk of CCSNe, spanning a remarkably broad range of absolute magnitudes, with ∼30 per cent of SLSNe-II arising from galaxies fainter than $M_{\rm nIR} \sim -14$. The detection of our faintest SLSN hosts increases the confidence that SLSNe-I hosts are distinct from those of LGRBs in star formation rate and stellar mass, and suggests that apparent similarities in metallicity may be due to the limited fraction of hosts for which emission line metallicity measurements are feasible. The broad range of luminosities of SLSN-II hosts is difficult to describe by metallicity cuts, and does not match the expectations of any reasonable UV-weighted luminosity function, suggesting additional environmental constraints are likely necessary to yield hydrogen rich SLSNe.

Key words: supernovae: general – galaxies: dwarf – galaxies: luminosity function, mass function – galaxies: starburst.

1 INTRODUCTION

During the past decade, time resolved, wide field, transient surveys such as the Panoramic Survey Telescope And Rapid Response System (Pan-STARRS; Kaiser & Pan-STARRS Team 2005), Palmomar Transient Factory (PTF; Law et al. 2009) and Catalina Real-time Transient Survey (CRTS, Drake et al. 2009), have revealed the extent of diversity amongst cosmic explosions showing that the optical transient sky exhibits a much broader range of events in both luminosity and duration than spanned by classical supernovae (SNe). These discoveries have largely been possible thanks to the unprecedented combination of depth, areal coverage and cadence of observations that are provided by such surveys, enabling order of magnitude increases in the number of transients recorded. This is combined with increasingly effective and sophisticated follow-up, that has allowed rare, hitherto unrecognised, populations of events to be uncovered, and sufficient numbers of events to be located to identify new populations, rather than just extreme outliers. Of particular interest are populations of highly luminous, but extremely rare SNe, peaking at magnitudes brighter than $M_V \sim -21$, a factor of ∼100 times brighter than the majority of core-collapse supernovae (CCSNe), and 10 times brighter at peak than SNe Ia. The achievement of such high luminosities during stellar collapse is likely a result of peculiar and poorly understood explosion mechanisms, through which we may shed light upon the exotic stars from which

⋆ E-mail: C.R.Angus@warwick.ac.uk

© 2016 The Authors
Published by Oxford University Press on behalf of the Royal Astronomical Society

Downloaded from http://mnras.oxfordjournals.org/ at California Institute of Technology on June 2, 2016

they originate. These Superluminous Supernovae (SLSNe) have been observed since at least the mid-1990's (Knop et al. 1999), but it is only in the past few years that sufficient numbers with detailed follow-up have become available, enabling them to be identified as a new population of events (Quimby et al. 2011a) complete with internal diversity similar to that seen in normal SNe, in particular the hydrogen-rich and -poor dichotomy (e.g. Gal-Yam 2012). In addition to their high luminosity, SLSNe also frequently exhibit long rise times, remaining brighter than the peak magnitude of most SNe for hundreds of days. Furthermore, they are extremely blue, in contrast to many SNe whose UV-light vanishes due to metal line blanketing shortward of ∼3000 Å in the rest frame. The combination of luminosity, longevity and blue colours makes them potentially powerful cosmological probes, visible, even with current technology, out to $z > 4$ (Inserra & Smartt 2014). Indeed, the most distant SNe detected[1] are of the SLSNe variety (Cooke et al. 2012; Howell et al. 2013).

SLSNe have been broadly classified in a similar manner to normal CCSNe, with hydrogen-poor and hydrogen-rich events being labeled Type-I and Type-II, respectively. Independent of these spectroscopic classifications, there is a suggested population of hydrogen-poor events whose light curves appear to be shaped by the rate of radioactive decay of nickel (^{56}Ni), Type-R (Gal-Yam 2012). At face value, if powered by standard radioactivity, the peak brightness of SLSN events imply the synthesis of several solar masses of ^{56}Ni during the explosion, a feat impossible in the most massive Galactic stars. This is due to ongoing mass-loss processes throughout their main-sequence lifetime that inhibit the growth of the core so that it cannot reach masses greater than ∼60 $M_\odot$ (Heger & Woosley 2002), the mass needed to synthesize the levels of ^{56}Ni implied by SLSNe peak magnitudes. This has led to suggestions that SLSNe originate from massive ($M > 100$ $M_\odot$), low metallicity stars, that may bear a strong resemblance to first generation, Population III stars (e.g. Gal-Yam et al. 2009). In this case, the explosion mechanism may be the complete destruction of the core in long sought after Pair Instability Supernovae (e.g. Rakavy & Shaviv 1967), whereby the production of electron–positron pairs within the core rapidly reduces internal pressure, causing the star to collapse. The resulting thermonuclear detonation disrupts the star entirely, leading to a luminous outburst. While mooted as a possible origin for many SLSNe, the Type-R events now seem the most likely candidates for such explosions.

However, this interpretation remains controversial with some arguing that they are simply a subset of Type-I SLSNe for which the similarity with a nickel decay is coincidental (Inserra et al. 2013; Nicholl et al. 2013). There are various proposed mechanisms for the production of such luminous outbursts. An extremely bright SN may be produced via the interaction of the SN shock wave with a dense shell of material expelled from the star during a prior evolutionary phase, shock heating the hydrogen-rich material, causing it to luminesce over a larger radius (the interaction model; Chevalier & Irwin 2011). Otherwise, the re-energizing of the SN shock wave via accretion on to a compact object or the spin-down of a magnetar could act as a mechanism to achieve the exceptional luminosity of SLSN events (the internal engine model; e.g. Kasen & Bildsten 2010; Dexter & Kasen 2013). These models have been proposed to explain the production of a reasonable subset of both the SLSN-II and SLSN-I events with moderately massive (∼20–40 $M_\odot$) stars, and evidence suggests that engines are active in at least some SLSNe both via detections of luminous X-rays (Levan et al. 2013), and detailed light curved modelling of SLSN events (Inserra et al. 2013; Nicholl et al. 2013, 2015).

Clearly, the progenitors of SLSNe remain poorly understood, as the current lack of constraints upon the properties of the SNe explosions make it difficult to ascertain which progenitor models are correct. A powerful way of tackling this problem is to study the host galaxies of these extreme cosmic explosions, and infer progenitor properties from the environments in which they form. This method has been used effectively to constrain the properties of progenitors of other types of transient. For example, early differences between SNe Ia and SNe II could be inferred from the presence of the former in ancient elliptical galaxies, while the latter arise exclusively in star-forming hosts. More recently, increasingly sophisticated approaches have been made to study both the luminosities and morphologies of the host galaxies of various transient types, along with their location within their hosts. Of particular relevance to SLSNe have been studies of the host galaxies of long duration gamma-ray bursts (LGRBs). These events, the only stellar collapse events whose luminosities exceed those of SLSNe (Bloom et al. 2009; Racusin et al. 2009), have been shown to arise primarily from the brightest regions of low mass, mainly low metallicity hosts (e.g. Fruchter et al. 2006; Savaglio, Glazebrook & Le Borgne 2009; Svensson et al. 2010; Perley et al. 2013). Such results imply that they arise from massive >40 $M_\odot$ low metallicity stars (e.g. Fruchter et al. 2006; Larsson et al. 2007; Raskin et al. 2008; Graham & Fruchter 2013). Similar constraints have been derived for 'normal' SNe, suggestive of an increasing mass spectrum from SN II → SN Ib → SN Ic (James & Anderson 2006; Kelly, Kirshner & Pahre 2008).

There have been several studies of the host galaxies of SLSNe. Neill et al. (2011) found the host galaxies of SLSNe to be exceptionally faint and blue, compared to a sample of field galaxies, although this study was limited by the depth of the observations (*GALEX* and Sloan Digital Sky Survey – SDSS), with the majority of the more recently discovered, better characterized, but more distant SLSNe yielding only upper limits for their hosts in the UV and optical. More recently Lunnan et al. (2014) carried out a survey of Type-I SLSN hosts, comparing the properties of their sample with those of the host galaxies of other core-collapse events such as 'normal' CCSNe and LGRBs. Their results implied that the hosts of SLSNe are less luminous and less metal rich than those of the general SNe population, but do exhibit comparable metallicities to the hosts of LGRBs, suggestive of similarities of progenitor between these two classes of event. Alternatively, the study of Mg and Fe absorption lines in handful of SLSN hosts by Vreeswijk et al. (2014), seems to suggest different progenitor paths for SLSN and LGRB events, due to the lower absorption strengths observed in SLSNe environments than in gamma-ray burst (GRB) hosts. A spectroscopic study of the hosts of SLSNe carried out by Leloudas et al. (2015) has shown the hosts of Type-I and Type-R events to possess extreme emission lines (Extreme Emission Line Galaxies), in contrast to SLSN-II hosts, which have comparatively softer radiation fields. The authors use this to support the notion of different progenitor systems for Type-I and Type-II events, advocating a massive, Population III-like progenitor for H-poor SLSNe. This is, however, contrary to the analysis of those who subscribe to a magnetar powered progenitor model (e.g. Inserra et al. 2013; Lunnan et al. 2014), for which a slightly less massive progenitor (>40 $M_\odot$; Davies et al. 2009) would suffice. Although the samples presented by Lunnan et al. (2014) and Leloudas et al. (2015) have limited overlap, their

[1] We exclude GRBs from this definition since while they are known to be core-collapse events we do not directly detect the SNe light beyond $z \sim 1$.

Downloaded from http://mnras.oxfordjournals.org/ at California Institute of Technology on June 2, 2016

distributions of metallicity are rather different, perhaps explaining the disparate conclusions.

In some cases it is possible to directly study the immediate environments of the SNe, and determine the stellar populations at the explosion sites. Spectroscopic measurements of the local ($\sim$ kpc) environment of SLSN PTF12dam (Thöne et al. 2015) have shown it to contain traces of recent starburst activity. Using the young stellar population and low metallicity of the region, the authors suggest a limit of >60 M$_\odot$ upon the progenitor system, seemingly in agreement with low metallicity, massive population-III like progenitors inferred from global host properties (although it should be noted that the light curve of this event can also be fit with CSM and magnetar powered models, see Chen et al. 2015).

However, a study of the fractional host light contained within locations of hydrogen-poor SLSNe within the ultraviolet carried out by Lunnan et al. (2015, a method used to great effect with the host galaxies for other core-collapse transients such as LGRBs and Type-Ic SNe to show a strong link between transient location and brightest star-forming regions within the host; Fruchter et al. 2006; Kelly et al. 2008; Svensson et al. 2010; Anderson et al. 2012) find that the locations of SLSNe-I are more concentrated on the light of their hosts than CCSNe, in which the probability of a CCSNe is roughly proportional to the surface brightness, but less concentrated than LGRBs. Given the strong link between stellar mass, stellar luminosity and stellar lifetime this could naturally be explained by longer lived, possibly lower mass progenitors for SLSNe-I.

In this paper, we present results from our survey of the hosts of SLSNe with the *Hubble Space Telescope* (*HST*) in the UV and nIR, complemented by a modest ground-based programme of optical observations. These observations provide a view of the ongoing star formation via deep rest-frame UV observations, as well as a handle on any older populations within the hosts substantially expanding the wavelength baseline with respect to earlier surveys. In this paper, we will focus on the broad-band photometric properties of the host galaxies, demonstrating their origin in extremely small, low mass, and likely metal poor, systems.

Throughout the paper we assume a standard Λ cold dark matter cosmology with $H_0 = 71$ km s^{-1} Mpc $^{-1}$ and $\Omega_{\rm M} = 0.27$ and $\Omega_{\rm vac} = 0.73$ (Larson et al. 2011). All reported magnitudes are given in the AB system and uncertainties are given at a 1σ confidence level, unless otherwise stated.

2 SAMPLE AND OBSERVATIONS

Here we use nIR and rest-frame UV observations of a sample of 21 SLSN host galaxies, within a redshift range of $0.019 < z < 1.19$ (SN 2006gy $\rightarrow$ SCP 06F6).

This *HST* sample (programme GO-13025; PI: Levan) comprised 21 targets, based on the sample of Neill et al. (2011), supplemented with luminous SNe from the literature (up to 2012 Jan). This selection pre-dated more detailed sample work, such as that by Gal-Yam (2012) which introduced a cut at $M_V < -21$ for inclusion in an SLSNe sample. In particular, several of the original sample, while significantly more luminous than typical SNe, were rather fainter than $M_V < -21$, based on the reported magnitudes and hence would be classed as luminous supernovae (LSNe) rather than SLSNe. However, it should be noted that early examples such as SN 1995av, SN 1997cy and SN 2000ei have extremely limited follow-up, and hence poorly know peak magnitudes, making their true nature uncertain. Conservatively we assign them as LSN in the absence of a detection of the SNe at a magnitude of $M_V < -21$. Additionally, the nature of SN 1997cy remains debated, and it now seems likely that it is a Type Ia-SNe interacting with a hydrogen-rich shell of circumstellar material (see Hamuy et al. 2003). Hence, we remove SN 1997cy from our sample of SLSNe for comparison with other populations. Other SNe that do not make the peak-luminosity threshold for SLSNe are classified as 'LSN', while the unambiguous SLSNe sample is then used for our analysis and conclusions. This yields a sample of 17 SLSNe and 4 LSNe. Unsurprisingly given the small contamination our conclusions are not significantly affected by the inclusion (or not) of LSNe.

Table 1 lists all the SNe targets used within this work and the distribution of redshifts for our sample is shown in Fig. 1. Fig. 1 also shows the redshift distributions of host samples of CCSNe discovered in GOODS (see also Dahlen et al. 2003; Fruchter et al. 2006; Svensson et al. 2010) and of GRBs at $z \lesssim 1.5$ (Fruchter et al. 2006; Savaglio et al. 2009; Svensson et al. 2010). We use these as a comparison sample of core-collapse events that should represent both all core-collapse systems creating a SNe (the GOODS CCSNe sample) and those occurring from only a restricted range of massive stars (probably those at low metallicity), represented by the GRBs. We implement a redshift cut at $z \sim 1.5$ on the GRB sample, in order to cover a comparable redshift range to our SLSNe, but do not include the many high-z GRBs whose host galaxies may differ because of the cosmological evolution of the galaxy population. It is now clear that low-z GRBs occur predominantly in smaller, lower luminosity galaxies than the more distant bursts, probably due to their metallicity dependence, combined with the shifting mass–metallicity relation with redshift (Perley et al. 2013, 2016; Schulze et al. 2015). Although this bias manifests itself predominantly below $z \sim 1$ (Perley et al. 2016) it is possible that should SLSNe and LGRBs both exhibit metallicity bias, but at a different critical metallicity, then we could confuse evolution in galaxy properties with differing environmental constraints. Indeed, the survey of SLSN-I host galaxies reported by Lunnan et al. (2014) does find some evidence for evolution, with lower-z SLSNe occurring in even smaller and lower luminosity galaxies. We note that within our pure SLSNe sample, 90 per cent of our SLSNe hosts lie at $z < 0.4$. Restricting our comparison samples to these lower redshifts does not impact the nature of our conclusions, but given the much smaller sample sizes would impact the statistical significance.

2.1 *HST* data

We obtained *HST* Wide Field Camera 3 (WFC3) images of the SLSN host galaxies for 21 hosts from of our sample. Observations were obtained in the rest-frame UV, probing the approximate rest-wavelength range of 2500–3500 Å and so we utilize *F*275*W* ($z < 0.1$), *F*336*W* ($0.1 < z < 0.3$) and *F*390*W* ($0.3 < z < 0.6$) filters. In each orbit we also switched from the UV to nIR channel in WFC3 to enable us to obtain short nIR exposures ($\sim$200 s), which despite their duration are competitive with much longer ground-based observations, reaching limits of $H_{\rm AB} \sim 25$ (3σ). In addition, we obtained deep observations of the well-studied (and initially mysterious) SLSN, SCP 06F6 (Barbary et al. 2009; Gänsicke et al. 2009) at $z = 1.19$. For this event, we obtained three orbits of exposure using Advanced Camera for Surveys (ACS)/WFC and *F*606*W*. A full log of observations is shown in Table 1.

Some of the host galaxies were undetected in these exposures, suggesting extremely faint absolute magnitudes ($M_{\rm nIR} > -15$). These were also targeted by a second programme (GO-13480; PI: Levan), which obtained deeper optical observations using ACS in *F*606*W* and WFC3 again in the nIR. Again a full log is shown in Table 1, alongside additional optical observations of other SLSNe

Downloaded from http://mnras.oxfordjournals.org/ at California Institute of Technology on June 2, 2016

Table 1. SLSN host sample used within this paper, listing positions, redshifts and observations used within this study. Optical imaging with r' filter obtained with the WHT, *B* and *R* band imaging using the Keck I 10m Telescope and additional *R* band imaging obtained with VLT.

SLSN	Class	z	RA (J2000)	Dec. (J2000)	UV Filter	T_{exp} UV (s)	Optical Band	T_{exp} opt. (s)	nIR Filter	T_{exp} nIR (s)	Ref.
SN1995av	LSN-IIn	0.300	02:01:41.34	+03 39 38.9	*F390W*	1808	r'	1500	*F160W*	206	[1]
SN1997cy	Ia/IIn	0.063	04:32:54.86	- 61:42:57.5	*F275W*	1832	–	–	*F160W*	206	[2]
SN1999as	SLSN-R	0.127	09:16:30.86	+13:39:02.2	*F336W*	2032	–	–	*F160W*	206	[3]
SN1999bd	SLSN-IIn	0.151	09:30:29.17	+16:26:07.8	*F336W*	2036	–	–	*F160W*	206	[3]
SN2000ei	LSN-II	0.600	04:17:07.18	+05:45:53.1	*F390W*	1808	r'	1500	*F160W*	206	[4]
SN2005ap	SLSN-I	0.283	13:01:14.83	+27:43:31.4	*F390W*	1804	r	240	*F160W*	206	[5]
SN2006gy	SLSN-IIn	0.019	03:17:27.06	+41:24:19.5	*F390W*	932	–	–	*F160W*	206	[6,7]
					F275W	846					
SN2006oz	SLSN-I	0.396	22:08:53.56	+00:53:50.4	–	–	r'	300	–	–	[8]
SCP06F6	SLSN-I	1.189	14:32:27.395	+33:32:24.83	*F606W*	8054	–	–	–	–	[9]
SN2007bi	SLSN-R	0.128	13:19:20.19	+08:55:44.3	*F336W*	1808	–	–	*F160W*	206	[10]
SN2008am	SLSN-IIn	0.234	12:28:36.30	+15:34:50.0	*F336W*	1808	–	–	*F160W*	206	[11]
SN2008es	SLSN-II	0.202	11:56:49.13	+54:27:25.7	*F336W*	1824	r'	1800	*F160W*	2812	[12, 13]
							F606W	5630			
							r	870			
							B	900			
SN2008fz	SLSN-IIn	0.133	23:16:16.60	+11:42:47.5	*F336W*	2032	r	1290	*F160W*	2612	[14]
							F606W	5236			
							B	1475			
SN2009jh	SLSN-I	0.349	14:49:10.09	+29:25:10.4	*F390W*	2044	r	240	*F160W*	2612	[15]
							F606W	5922			
PTF09atu	SLSN-I	0.501	16:30:24.55	+23:38:25.0	*F390W*	2036	r'	1500	*F160W*	206	[15]
PTF09cnd	SLSN-I	0.258	16:12:08.96	+51:29:16.0-	*F390W*	2224	r'	1500	*F160W*	206	[15]
SN2010gx	SLSN-I	0.230	11:25:46.71	- 08:49:41.4	*F390W*	1808	–	–	*F160W*	206	[8,15]
PTF10hgi	LSN-I	0.10	16:37:47.00	+06:12:32.3	–	–	r'	1500	–	–	[16]
PTF10vqv	SLSN-I	0.45	03:03:06.80	-01:32:34.9	–	–	r'	1500	–	–	[17]
SN2011ke	SLSN-I	0.385	13:50:57.77	+26:16:42.8	*F336W*	2044	–	–	*F160W*	206	[16]
SN2011kf	SLSN-I	0.245	14:36:57.53	+16:30:56.7	*F336W*	2036	–	–	*F160W*	206	[16]
PTF11dsf	SLSN-IIn	0.143	16:11:33.55	+40:18:03.5	*F390W*	1832	r'	900	*F160W*	206	[18]
PTF11rks	LSN-I	0.190	01:39:45.51	+29:55:27.0	*F336W*	1804	r'	1800	*F160W*	206	[16]
SN2012il	SLSN-I	0.175	09:46:12.91	+19:50:28.7	*F336W*	2036	–	–	*F160W*	206	[16]

References: [1] Richardson et al. (2002) (classification uncertain), [2] Hamuy et al. (2003), [3] Gal-Yam (2012), [4] Schmidt et al. (2000), [5] Quimby et al. (2007), [6] Smith et al. (2007), [7] Ofek et al. (2007), [8] Leloudas et al. (2012, 2015), [9] Barbary et al. (2009), [10] Gal-Yam et al. (2009), [11] Chatzopoulos et al. (2011), [12] Miller et al. (2009), [13] Gezari et al. (2009), [14] Drake et al. (2010), [15] Quimby et al. (2011a), [16] Inserra et al. (2013), [17] Quimby et al. (2010), [18] Quimby et al. (2011b). Note that PTF10hgi and PTF11rks are also sometimes referred to by their IAU designations of SN 2010md and SN 2011kg respectively.

in our sample obtained from the ground with the William Herschel Telescope (WHT) and the Very Large Telescope (VLT).

We stack and process our images within PYRAF using AstroDrizzle software (Fruchter & Hook 2002). WFC3/UVIS and ACS images we drizzle to a final pixel scale of 0.025 arcsec, while for the nIR images we retain the native 0.13 arcsec pixel scale due to the lack of dithering. Within the UV data set, images are subject to greater charge transfer efficiency (CTE) losses, which arise due to inefficient transfer of charge between pixels during CCD readout, a consequence of cumulative radiation damage in a low Earth orbit environment (Bourque et al. 2013). To mitigate against this, all early images taken under programme GO-13025 utilized a pre-flash to fill charge traps, while in the latter observations we additionally moved the sources to the corners of the chip to minimize the number of transfers. The final individual images were then cleaned for CTE tails using the method of Anderson & Bedin (2010) prior to drizzling.

The UV images were re-drizzled again to match the plate scale of the nIR imaging (0.13 arcsec pixel^{-1}). Though this lowers the resolution of the image, the technique allows for easier detection of low surface brightness features, and for a direct comparison between the nIR and UV imaging.

Inclusive of our later, deeper imaging, we detected 18/21 of our *HST* imaged SLSNe in our rest-frame UV imaging, and 19/20 in the nIR imaging. The hosts of some of the undetected SLSNe in our initial observations were recovered in the deeper exposures. Hence, we have host detections in at least a single band for ∼90 per cent of our *HST* observed sample (all SLSNe excluding PTF09atu).

2.2 Astrometry

The majority of SLSNe from our sample possess discovery locations such that the SN position lies on, or close to, an underlying host detected within our *HST* imaging. Where possible, we perform initial astrometry measurements using discovery imaging where the SNe are as close as possible to maximum light. Imaging used in this procedure is described in Table A1. Astrometric measurements were carried out by aligning the discovery images by World Coordinate System (WCS) for an initial approximation. Using routine IRAF tasks we determine the [*x*,*y*] centres of multiple matching sources in both discovery and *HST* fields, using point sources where available. Using IRAF tasks GEOMAP and GEOXYTRAN, we map and transform between coordinate systems for the two images, before transforming the [*x*,*y*] co-ordinates for the SN within the discovery image to the

Downloaded from http://mnras.oxfordjournals.org/ at California Institute of Technology on June 2, 2016

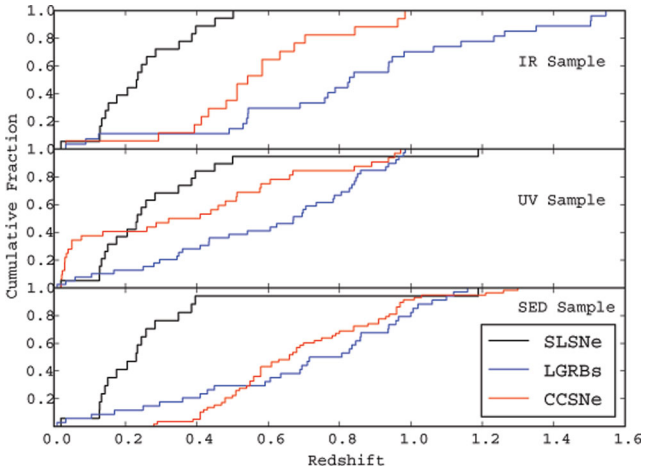

Figure 1. Redshift distribution of SLSN hosts used for comparisons in this work. We compare rest-frame IR (top) and UV (middle) properties, as well as masses and SFRs derived from SED fitting (lower panel). Since these different diagnostics are available for only a fraction of each of our comparison samples the global redshift distribution is less appropriate. Hence we show the redshift distribution for each sample separately. The SLSN host galaxies are typically at lower redshift ($z < 0.5$) than the GRBs, or than the GOODS CCSNe samples to which we wish to compare. The possible impacts of this selection, and consideration of alternatives are presented in Section 5.

corresponding pixel within our *HST* imaging. This allows the SN position to be determined within the *HST* imaging. For four of our *HST* hosts for which discovery images were unavailable (namely SN 1997cy, SN 1999bd, SN 2000ei and SN 2011kf), we can only localize the SN position to the discovery RA and Dec., correcting for small offsets in *HST*'s WCS solution by aligning it with 2MASS point sources.

We note that in the case of three SLSNe from our sample, initial astrometric measurements create some ambiguity in the identification of the real host. For SN 2000ei the presence of two galaxies within ∼1 arcsec of the SN position precludes its unique identification. We test the chance probability of association ($P_{\rm chance}$) that an unrelated galaxy of the same optical magnitude or brighter would be found within the given offset from the apparent host for SN 2000ei from each of these nearby galaxies, using the method outlined within Bloom, Kulkarni & Djorgovski (2002). We adopt the host to the south-west of the SN location, which has the lowest $P_{\rm chance}$ value ($= 4.0 \times 10^{-3}$), as the true host to SN 2000ei.

Initial astrometric measurements for SN 2006gy suggest that the SN location is coincident with an unresolved 'knot' of radiation approximately ∼1 arcsec from the centre of NGC 1260, suggestive of perhaps a much smaller host satellite to the larger galaxy or that the SN continues to contribute strongly, even 8 yr after the SN detection (see Fig. 4). To test this we perform relative astrometry compared to an archival image of the SN, taken in 2008 November using the Wide Field and Planetary Camera 2 (WFPC2) in the *F*450*W* band (GO-10877, PI: Li). We find the SN position to be consistent with the centre of the source seen in our observations with a 0.08 arcsec error circle.

Subtraction of a point spread function reveals some possible features around the SN position, however, these could be faint features within the disc of NGC 1270, rather than extension of the source at the location of SN 2006gy. The source magnitude in our imaging of $F390W(\mathrm{AB}) = 22.6 \pm 0.1$ corresponds to an absolute magnitude of ~ -11.7, while if we assume that the source is unresolved (or at least the majority of the light arises from a very compact region) then the size is <30 pc. This size is typical of a globular cluster, but the magnitude in blue light is too bright (e.g. Harris 1996). If it were a dwarf galaxy it would be relatively faint (e.g. McConnachie 2012), but unusually compact. In this case it may be an ultracompact dwarf, a magnitude fainter than the densest known example, M85-HCC1 (Sandoval et al. 2015), but comparable in size. Given the astrometric coincidence with the SN position it is then perhaps more likely the light continues to be dominated by SN emission (see also Miller et al. 2010; Fox et al. 2015), although in this case the minimal fading over the course of several thousand days is puzzling and also requires unusual explanations (Fox et al. 2015). Further observations will clearly be needed to distinguish between these possibilities. However, as the source is relatively faint, it does not significantly contribute to the photometric measurements of the host galaxy, and so does not impact our conclusions drawn for it.

In the case of SN 2009jh, the SN apparently lies to the north-east of the host detected in deeper nIR imaging. We determine the $P_{\rm chance}$ value of the apparent host of SN 2009jh, which we find to be 0.038 within an offset radius of 0.99 arcsec (from the host half light radius and the SN's projected offset from the host centroid), indicating that for the optical depth reached within our ACS imaging, the probability of the event being associated with another galaxy is low, but not especially so. Indeed, averaged over 20 hosts, we would expect a chance alignment with a sample of this brightness. We assign this nearby galaxy as the true host of SN 2009jh.

We note that although the inclusion or exclusion of hosts SN 2006gy and SN 2009jh does not dramatically impact the results presented here, the host of SN 2006gy is the most luminous host in our sample by some margin, and so assigning it to a fainter satellite would result in some changes to the range of our distribution of SLSNe-II host luminosities.

A mosaic of our nIR and UV observations are shown in Figs 2 and 3, respectively, (and our imaging of SN 2006gy in three bands shown within Fig. 4) with the approximate location of the SN marked in each case (the detailed locations and statistics of the SLSNe positions within their hosts will be considered in forthcoming work, Angus et al., in preparation).

2.3 Ground-based observations

We supplement our *HST* observations with our own various ground-based programmes. We carried out a service mode programme using Auxiliary Camera (ACAM) on the WHT to obtain relatively shallow optical imaging (∼1500–1800s of SDSS r' band) for a small sample of SLSN hosts (namely SN 1995av, SN 2000ei, SN 2006oz, SN 2008es, PTF09atu, PTF09cnd, PTF10hgi, PTF10vqv, PTF11dsf and PTF11rks).

We acquired *R*-band imaging of three galaxies from our sample (namely the hosts of SN 2005ap, SN 2008fz and SN 2009jh) using the FOcal Reducer and low dispersion Spectrograph (FORS2; Appenzeller et al. 1998) on the VLT during the nights of 2013-08-31, 2014-01-24 and 2014-02-01. We obtained 239 s of *R*-band imaging for each host, reducing the images using standard procedures within IRAF. We recover faint unresolved detections of each host galaxy within our imaging. The calculated aperture magnitudes obtained for our spectral energy distribution (SED) fitting are provided within Table 2.

We acquired deep optical imaging of the two faintest targets in the low-z sample (SN 2008es and SN 2008fz) using the Low Resolution Imaging Spectrometer (Oke et al. 1995) on the the Keck I 10 m telescope, during the night of 2013-12-04. We obtained 900 s of *B*-band imaging and 870 s of *R*-band imaging of the

Downloaded from http://mnras.oxfordjournals.org/ at California Institute of Technology on June 2, 2016

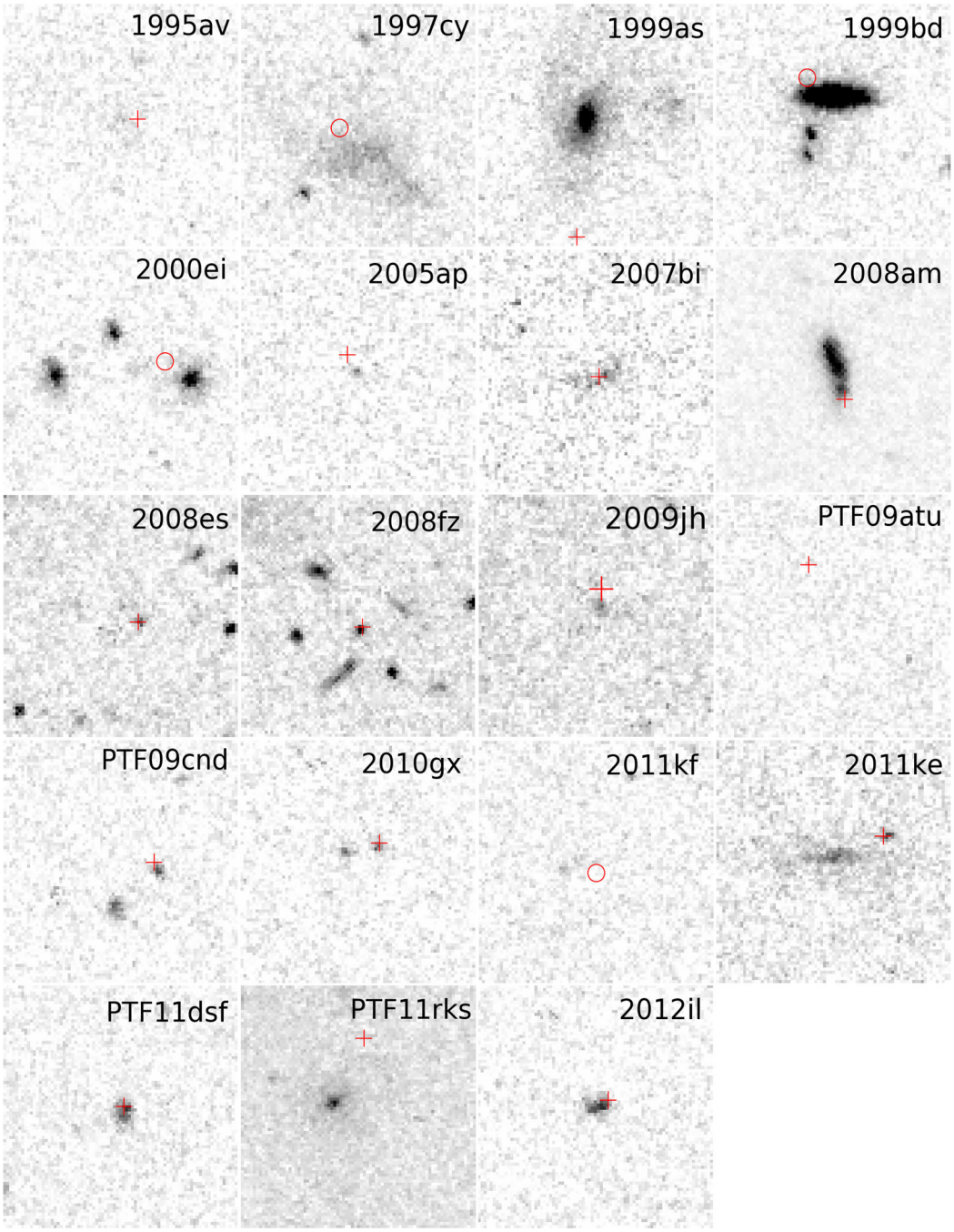

Figure 2. Host galaxies of SLSNe imaged in the nIR with *HST* GO-13025 and GO-13480. Images (bar SN 2006gy – see Fig. 4) are scaled to 10 arcsec $\times$10 arcsec and approximate SN positions are marked with red crosses where astrometry has been carried out, or circles located at the discovery coordinates of the SNe where discovery images were not available.

host of SN 2008es, and 1475 s of *B*-band imaging and 1290 s of *R*-band imaging of the host of SN 2008fz. Images were reduced using standard procedures via an automated pipeline (LPipe). We recover faint, unresolved detections of the host galaxy of both targets in both filters, and calculate aperture magnitudes for our SED analysis.

3 PHOTOMETRY

Photometry was performed using one of two different methods, dependant upon the appearance of the host galaxy within the *HST* imaging. Where possible we used the automatic detection and extraction package, Source Extractor (here after SExtractor; Bertin & Arnouts 1996), for which the program parameters were adjusted accordingly for each host to optimize its detection and extraction. Here, we applied a surface brightness signal-to-noise cutoff of two per pixel for nIR images and one for UV images, in order to include faint surface brightness features. We report measured host magnitudes as MAG_AUTO values which attempt to account for additional light outside of the notional aperture. Several galaxies show a light distribution dominated by individual bright knots in ultraviolet imaging, and the deblending parameters were adjusted

Downloaded from http://mnras.oxfordjournals.org/ at California Institute of Technology on June 2, 2016

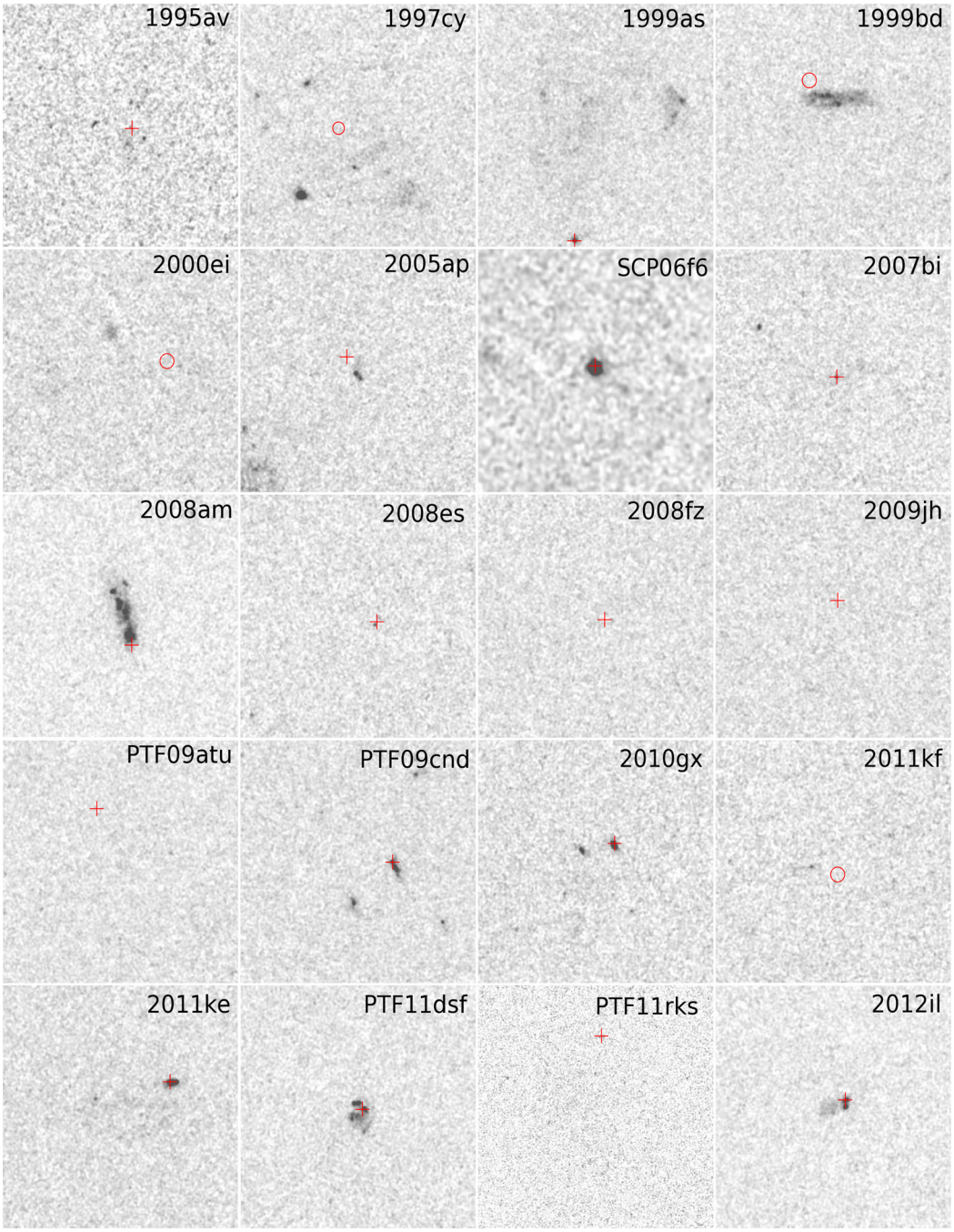

Figure 3. Host galaxies of SLSNe imaged in the UV with *HST* GO-13025. Images (bar SN 2006gy – see Fig. 4) are scaled to 10 arcsec ×10 arcsec and drizzled to nIR pixel scale to highlight low surface brightness features. Approximate SN positions are marked with red crosses where astrometry has been carried out, circles located at the discovery coordinates of the SNe where discovery images were not available.

for each host to ensure it was not broken into multiple components. For this work the nIR images were used to determine which UV components should be included in the analysis, as these bands are dominated by a smoother light profile arising from older stars. Zeropoints for each filter were taken from the Space Telescope Science Institute (STScI) WFC3 handbook (Dressel 2012).

We also utilize straightforward aperture photometry, setting large apertures to encompass the majority of the light of the galaxy, and determining the background via the use of a large number (>20) of sky apertures. This technique gave results consistent with those determined via SExtractor, and was used to obtain 3σ limits where necessary. In these cases we apply an aperture correction determined by the estimated encircled energy curves of WFC3 detectors (Dressel 2012). In the case of a detection in one band but no detection in another, the size of the aperture used to determine the upper limit was set equal to that used to measure the magnitude in the band where the source was detected.

Additional photometry of hosts imaged using the WHT and VLT in r' and Johnson–Morgan R bands, respectively, was carried out in a like manner to the *HST* images, applying a surface signal-to-noise cutoff of one per pixel before extraction. Photometry of galaxies on ground based images was carried out relative to SDSS

Downloaded from http://mnras.oxfordjournals.org/ at California Institute of Technology on June 2, 2016

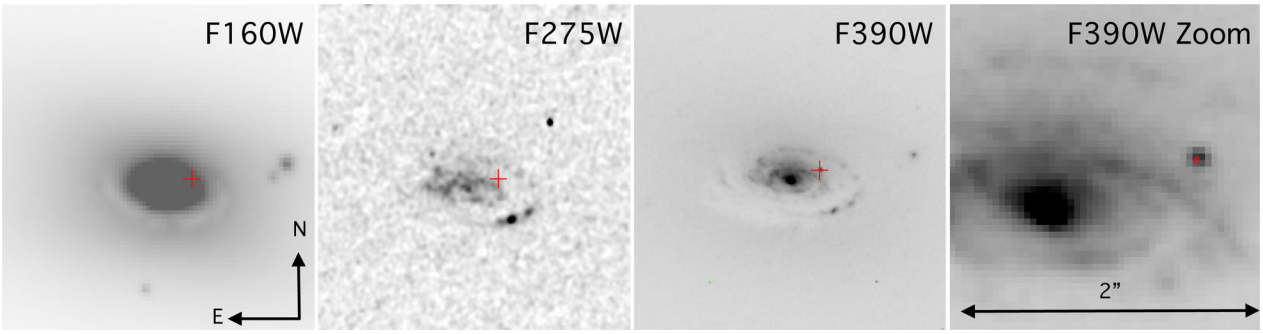

Figure 4. Host of SN 2006gy detected in *F*160*W* (first panel), *F*275*W* (second panel) and *F*390*W* (third panel). Images are scaled to 10 arcsec × 10 arcsec. The SNe location, determined from astrometric measurements from late time imaging with WFPC2, is marked in red. We draw attention to a possible satellite to the larger host, coincident with the SNe location, revealed within our *F*390*W* imaging. To highlight this we provide a 2 arcsec × 2 arcsec image zooming in on this region and the central bulge in the fourth panel, where the SNe position is marked by a 0.08 arcsec error circle.

Table 2. Apparent and absolute magnitudes of SLSN hosts observed with *HST* in nIR (*F*160*W*), rest-frame UV (*F*275*W*, *F*336*W* or *F*390*W*) and optical bands. Optical photometric properties of a subset of this sample as observed with [a]WHT (r'), [b]VLT (*R* band) and [c]*HST* ACS (*F*606*W*). We also present apparent r_{80} sizes of our *HST* SLSN hosts as detected within WFC3 *F*160*W* imaging. Optical imaging key: [a]r' band, [b]*R* band, [c]*B* band.

SLSN	m_{UV} AB mag	M_{UV} AB mag	$m_{optical}$ AB mag	$M_{optical}$ AB mag	m_{nIR} AB mag	M_{nIR} AB mag	r_{80} (kpc)	r_{80} (arcsec)
SN1995av	24.97 ± 0.32	−15.82 ± 0.32	23.77 ± 0.19[a]	−16.96 ± 0.19[a]	23.17 ± 0.27	−17.51 ± 0.27	10.66 ± 3.07	2.41 ± 0.69
SN1997cy	21.14 ± 0.21	−16.17 ± 0.21	–	–	20.19 ± 0.03	−16.98 ± 0.03	3.29 ± 1.10	2.75 ± 0.91
SN1999as	21.15 ± 0.10	−17.70 ± 0.10	–	–	19.19 ± 0.03	−19.55 ± 0.03	6.81 ± 2.39	3.03 ± 1.07
SN1999bd	21.85 ± 0.06	−17.40 ± 0.06	–	–	18.779 ± 0.003	−20.349 ± 0.003	2.95 ± 1.02	1.13 ± 0.39
SN2000ei	23.81 ± 0.21	−19.29 ± 0.21	22.67 ± 0.14[a]	−20.07 ± 0.14[a]	20.90 ± 0.03	−21.44 ± 0.03	6.55 ± 2.00	0.98 ± 0.30
SN2005ap	24.32 ± 0.09	−16.24 ± 0.09	23.64 ± 0.27[a]	−16.90 ± 0.27[a]	23.48 ± 0.36	−17.05 ± 0.36	3.23 ± 0.85	0.76 ± 0.20
SN2006gy	19.86 ± 0.01	−15.55 ± 0.01	–	–	11.951 ± 0.001	−22.661 ± 0.001	3.69 ± 2.11	9.70 ± 5.56
SN2006oz	–	–	24.09 ± 0.26[a]	−16.83 ± 0.26[a]	–	–	–	–
SCP06F6	27.88 ± 0.20	−15.88 ± 0.20	–	–	–	–	–	–
SN2007bi	23.83 ± 0.28	−15.03 ± 0.28	–	–	22.07 ± 0.18	−16.68 ± 0.18	2.62 ± 0.77	1.16 ± 0.34
SN2008am	21.20 ± 0.026	−19.00 ± 0.026	–	–	19.48 ± 0.006	−20.63 ± 0.006	4.31 ± 1.44	1.17 ± 0.39
SN2008es	>25.32	>−14.526	25.96 ± 0.20[b]	−13.86 ± 0.20[b]	26.85 ± 0.40	−12.95 ± 0.40	1.19 ± 0.23	0.36 ± 0.07
			26.96 ± 0.25[c]	−12.85 ± 0.25[c]				
SN2008fz	26.73 ± 0.55	−12.28 ± 0.55	25.58 ±0.19 [b]	−13.33 ± 0.19[b]	25.18 ± 0.06	−13.66 ± 0.06	0.87 ± 0.18	0.37 ± 0.08
			26.17 ± 0.22[c]	−12.81 ± 0.22[c]				
SN2009jh	>25.92	>−15.139	25.46 ± 0.07[b]	−15.59 ± 0.07[b]	25.30 ± 0.15	−15.71 ± 0.15	2.71 ± 0.63	0.55 ± 0.13
2010gx	23.96 ± 0.04	−16.24 ± 0.04	–	–	23.17 ± 0.15	−16.90 ± 0.15	1.84 ± 0.46	0.51 ± 0.13
PTF09atu	>25.47	>−16.533	>23.14[a]	>−18.79[a]	>23.39	>−18.452	–	–
PTF09cnd	24.01 ± 0.05	−16.40 ± 0.05	23.60 ± 0.04[a]	−16.768 ± 0.04[a]	22.56 ± 0.12	−17.76 ± 0.12	3.11 ± 0.89	0.78 ± 0.22
PTF10hgi	–	–	22.05 ± 0.06[a]	−16.329 ± 0.06[a]	–	–	–	–
PTF10vqv	–	–	23.33 ± 0.12[a]	−18.392 ± 0.12[a]	–	–	–	–
2011ke	23.12 ± 0.03	−15.92 ± 0.03	–	–	23.21 ± 0.14	−15.78 ± 0.14	5.17 ± 1.48	2.08 ± 0.60
2011kf	24.51 ± 0.38	−15.78 ± 0.38	–	–	24.06 ± 0.40	−16.14 ± 0.40	1.24 ± 0.27	0.33 ± 0.07
PTF11dsf	22.88 ± 0.04	−18.38 ± 0.04	22.04 ± 0.11[a]	−19.204 ± 0.11[a]	21.81 ± 0.07	−19.41 ± 0.07	3.48 ± 0.98	0.67 ± 0.19
PTF11rks	22.43 ± 0.16	−17.38 ± 0.16	20.95 ± 0.25[a]	−18.77 ± 0.25[a]	20.69 ± 0.06	−18.96 ± 0.06	5.55 ± 1.77	1.77 ± 0.57
SN2012il	22.78 ± 0.06	−16.75 ± 0.06	–	–	21.82 ± 0.06	−17.63 ± 0.06	1.89 ± 0.53	0.64 ± 0.18

observations of the same field, and is given in the r' band. We correct all our photometry for Galactic extinction using the Milky Way dust maps of Schlafly & Finkbeiner (2011) (via the NASA/IPAC Infrared Science Archive[2]) for the appropriate image filter.

3.1 Comparison samples

While the properties of the SLSN hosts themselves are of interest, they are most diagnostic when compared to other classes of extragalactic transient whose progenitors are better understood. To this end, we employ a comparison sample of LGRB and CCSN[3] host galaxies. In principle, CCSNe should trace all core-collapse events, although the mass function means they will be dominated by stars at the lower mass end (∼8 $M_\odot$ to ∼25 $M_\odot$). There also remains a possibility that some very massive stars can undergo core collapse without yielding a LSNe (e.g. Smartt 2009; Ugliano et al. 2012; Kochanek 2014) such that CCSNe samples might only provide a census of lower mass core collapsing stars (e.g. $8 < M_* < 20\,M_\odot$). Indeed, constraints from explosion parameters have shown the majority of CCSNe to be consistent with lower mass progenitors,

[2] http://irsa.ipac.caltech.edu/applications/DUST/

[3] Here, we use CCSNe to define all core-collapse events, including SN Ib, Ic, II and their various subtypes. Where appropriate and possible, we specify the SN type.

Downloaded from http://mnras.oxfordjournals.org/ at California Institute of Technology on June 2, 2016

as opposed to more massive Wolf–Rayet stars (Cano 2013; Lyman et al. 2016) GRBs likely represent a population with rather larger initial masses (Larsson et al. 2007; Raskin et al. 2008). LGRBs are now known to be associated with the core collapse of massive stars, and broad line SN Ic are near ubiquitously associated with low-z events (where such signatures can be seen; Hjorth et al. 2012). When compared to the hosts of CCSNe they are generally smaller and of lower luminosity, consistent with an origin in galaxies of lower metallicity (Fruchter et al. 2006; Svensson et al. 2010). In relatively local examples, where spatially resolved gas phase metallicities can be obtained, these indeed appear to be lower for GRBs than for CCSNe, even in cases where the luminosity of the galaxy is relatively high (i.e. the GRB host galaxies lie off the mass–metallicity relation; Modjaz et al. 2008; Graham & Fruchter 2013). Hence, comparing the hosts of SLSNe to these events allows us to test the large-scale environments of SLSNe against those of the bulk core-collapse population and a subset which appears to derive largely from massive stars at lower metallicity, although we note that agreement on this matter is not complete (e.g. Podsiadlowski, Joss & Hsu 1992; Eldridge, Izzard & Tout 2008; Smartt 2009; Drout et al. 2011). By exploiting both LGRB and CCSN host samples we can ascertain if there is a strong metallicity dependence in SLSN production, and if this is more or less extreme than that observed in GRB hosts.

The observed samples are undoubtedly biased against highly dusty lines of sight such that the most dusty examples are missed. This effect has been well studied in GRBs (e.g. Jakobsson et al. 2006; Fynbo et al. 2009), and the inclusion of dusty sight lines does apparently extend the GRB host mass function to higher masses than if they are excluded (e.g. Perley et al. 2013). However, the effect below $z \sim 1.2$, where our comparisons to SLSNe are conducted, is small, with very few dusty massive systems (Perley et al. 2015, 2016; although see Stanway et al. 2015). The impact on SNe detection may be even larger given their fainter peak magnitudes and uniquely optical selection.

Tables A2, A3 and A4 list the names, locations and redshifts of the host galaxies for direct photometric comparison. We make our own photometric measurements for hosts with available *HST* rest-frame UV or nIR imaging, and draw from literature elsewhere.

Our LGRB host sample contains events at $z \lesssim 1.2$ (for broad matching of the SLSNe redshift distribution, and comparable sample size). Rest-frame UV observations are obtained from the literature (in particular utilizing the GHostS project Savaglio et al. 2009, for other references see Table A4). nIR observations are obtained from GHosts, and also from our *HST* snapshot programme GO-12307; PI: Levan, Lyman et al., in preparation).

Our CCSNe host sample is based on that detected in the rolling SNe searches of the GOODS field (Dahlen et al. 2003; Fruchter et al. 2006; Riess et al. 2007; Strolger, Dahlen & Riess 2010; Svensson et al. 2010). These tiled the GOODS field repeatedly in the *F*850*LP* filter, with a cadence of ∼45 d, primarily chosen to locate SNe Ia at $z > 1$. However, this search also provides an untargeted and highly sensitive moderate redshift ($0.1 < z \lesssim 1$) survey for core-collapse events. Subsequently, the GOODS field has been observed in the nIR with both Near Infrared Camera and Multi-Object Spectrometer (NICMOS) and WFC3, and more recently in the blue using ACS and WFC. We use these images to obtain nIR magnitudes for the CCSN hosts, and for rest-frame UV magnitudes where field coverage and redshifts allow, performing photometry as described above for the SLSNe population.

Due to restrictions in field coverage and probed rest-frame wavelength from the GOODS UV field imaging, we supplement our CCSNe host comparison sample with that of Sanders et al. (2012), which provides an untargeted, albeit typically low redshift, sample of stripped envelope SNe hosts. For these hosts we draw upon literature values to determine their rest-frame UV brightness.

4 DETERMINING THE PHYSICAL PARAMETERS

The redshifts of all of our sample of both SLSNe and comparison objects are known, and hence we can compare the physical properties of the galaxies. Of particular use can be a simple comparison of observed properties to physical properties over a similar redshift range, especially in cases for which SED coverage is poor. In particular, we can compare the absolute magnitudes at UV and nIR wavelengths, using these as proxies for star formation rate (SFR) and stellar mass, respectively.

We apply SED fitting to all of our hosts, to constrain masses, ages and SFRs. We also measure the sizes of the host galaxies, specifically the radius within which 80 per cent of their light is contained (following Fruchter et al. 2006; Svensson et al. 2010).

4.1 SED fitting

We have photometry from rest-frame nIR to near UV in all cases, with an extension to the mid-IR for brighter hosts, which allows us to fit template SEDs. To do this we supplement our own photometric measurements with those from other public data and literature. We use SDSS images (Ahn et al. 2012) to extract optical photometry for our hosts using the same techniques applied to our own ground-based imaging, in some cases this is supplemented with observations with Catalina Real-time Transient Survey (CRTS; Drake et al. 2009), and additionally use mid-IR observations from *WISE*. Finally, we also utilize published photometry of individual SLSN host galaxies from Germany et al. (2000), Quimby et al. (2007), Barbary et al. (2009), Neill et al. (2011), Hudelot et al. (2012), Leloudas et al. (2012) and Lunnan et al. (2014) to complete our SEDs. For all photometry, we utilize the MAG_AUTO function within SExtractor, which models and accounts through fitting Kron-like elliptical apertures to the source, in order to minimize any differences in the fraction of host light across different bands.

The acquisition of both nIR and UV data points allows us to simultaneously fit both masses and SFRs, which when combined with the depth of the imaging provides better constraints upon the blue and red ends of spectra when fitting, achieving more realistic estimates of host properties than previous SED fitting attempts. The broad-band observations are fitted against the template model chosen to derive masses, ages and SFRs for these hosts, a more detailed outline of which can be found within Perley et al. (2013). Here we assume a mass-dependent metallicity and a host ionization parameter of 4×10^7, except in the case of SN 2011kf and SN 2011ke, as in both of these SED's there was an observable excess of flux within the filters corresponding to rest-frame O[III] or H α lines when compared to a fit with no nebular emission. In these cases, we draw this parameter from the previous spectroscopic studies of Lunnan et al. (2014) and Leloudas et al. (2015).

4.2 Luminosity diagnostics

Whilst SED fits allow us to determine the properties of host galaxies to a relatively high degree of precision, the constraints of an SED fit are strongly dependent upon the number and wavelength range of bands used to fit the template spectra. The properties derived

Downloaded from http://mnras.oxfordjournals.org/ at California Institute of Technology on June 2, 2016

are also highly sensitive to star formation history adopted during the fitting procedure. For simplicity, and for direct comparison with previous work we therefore also consider nIR and UV rest frame luminosities as direct proxies for the stellar mass and SFR.[4] To do this we utilize the relations used in Savaglio et al. (2009) for stellar mass, namely that

$$\log M_* = -0.467 M_{\rm nIR} - 0.179. \quad (1)$$

We can also directly convert our rest-frame UV luminosities into SFRs as per Kennicutt (1998);

$$\mathrm{SFR}(\mathrm{M}_\odot\ \mathrm{yr}^{-1}) = 1.4 \times 10^{-28} L_\nu, \quad (2)$$

where L_ν is in cgs units of erg s^{-1} Hz^{-1} in the rest-frame wavelength range from 2500 to 3500 Å, a region in which all our UV observations lie. This relation assumes a constant star formation over a 100 Myr period with a specified initial mass function. Utilizing both mass and SFR we can also calculate a specific SFR, $\Phi = \frac{\mathrm{SFR}}{M_*}$. These values generally give results comparable to those from our direct SED fitting.

Finally, in addition to straightforward photometry, SExtractor also can be used to ascertain the fractional light radii of host galaxies using the FRAC_LIGHT parameter (Bertin & Arnouts 1996), which fits an isophotal profile to a source then measures the relative size of the source in pixels, later converted into kiloparsecs using the plate scale. We use the common LGRB host diagnostic of radii containing 80 per cent of the total flux from the host (r_{80}) within the nIR $F160W$ images.

Errors for the SExtractor measurement of r_{80} in pixels for the hosts were estimated by modelling the capability of SExtractor to detect the full radial profile of a source at given magnitude and redshift as a function the image noise. An artificial field of objects were generated using IRAF routines, with artificial galaxies specified to span a similar apparent magnitude and surface brightness range to our host galaxies in the $F160W$ band. The discrepancy between specified object size and that measured by SExtractor was measured, with different levels of simulated noise, suggesting that significant errors can arise for sources close to the noise limit. These errors are provided in Table 2, alongside our r_{80} estimates.

5 RESULTS

Below we first present the measured nIR and UV luminosities of the host galaxies, and consider the implications these results have when treated as proxies for stellar mass and SFR, respectively, before evaluating the derived SED properties of our hosts, and their physical sizes. We then compare these to our comparison samples. In the majority of cases it is apparent that the SLSNe hosts bear little similarity with any other core-collapse host population, being both fainter and smaller, we consider the implications of this in Section 6.

The photometric UV, optical and nIR magnitudes of the LSN and SLSN host sample considered within this work are presented in Table 2, and the derived UV and nIR host properties from SED fitting of these hosts are presented in Table 3. The direct photometric measurements and derived properties of our chosen LGRB and CCSN comparison samples are presented for nIR and UV observations within Tables A2, A3 and A4, respectively.

[4] In figures in which the main x-axis shows an observed absolute magnitude, the upper axis therefore shows the mass/SFR inferred from these proxies, while figures showing physical parameters are those derived from SED fits.

Table 3. Properties of SLSN hosts derived from SED fitting. Uncertainties presented here are those associated with photometric errors only and do not include systematic uncertainties related to the fitted SED models. Objects marked * are detected within only one band. Mass errors provided for these objects represent for the upper and lower bound we can place upon these hosts.

SLSN	SFR ($\mathrm{M}_\odot$ yr^{-1})	M_* ($\times 10^9$ $\mathrm{M}_\odot$)
SN1995av	$0.201\ ^{+0.063}_{-0.077}$	$0.578\ ^{+0.270}_{-0.192}$
SN1997cy	$0.170\ ^{+0.207}_{-0.030}$	$0.255\ ^{+0.042}_{-0.216}$
SN1999as	$0.610\ ^{+0.014}_{-0.006}$	$2.197\ ^{+0.396}_{-0.000}$
SN1999bd	$0.412\ ^{+1.030}_{-0.259}$	$10.494\ ^{+1.339}_{-2.073}$
SN2000ei	$9.597\ ^{+3.511}_{-0.000}$	$0.863\ ^{+0.175}_{-0.000}$
SN2005ap	$0.090\ ^{+0.017}_{-0.016}$	$0.287\ ^{+0.107}_{-0.097}$
SN2006gy	$0.000\ ^{+0.000}_{-0.000}$	$153.280\ ^{+6.251}_{-6.463}$
SN2006oz	$0.069\ ^{+0.032}_{-0.024}$	$0.893\ ^{+0.131}_{-0.075}$
SCP06F6*[a]	$0.136\ ^{+0.028}_{-0.025}$	$0.010\ ^{+0.000}_{-0.000}$
SN2007bi	$0.048\ ^{+0.006}_{-0.009}$	$0.136\ ^{+0.097}_{-0.053}$
SN2008am	$2.018\ ^{+0.001}_{-0.002}$	$5.637\ ^{+0.018}_{-0.047}$
SN2008es	$0.007\ ^{+0.001}_{-0.001}$	$0.006\ ^{+0.005}_{-0.005}$
SN2008fz	$0.009\ ^{+0.001}_{-0.001}$	$0.017\ ^{+0.001}_{-0.001}$
SN2009jh*	$0.030\ ^{+0.000}_{-0.000}$	$0.068\ ^{+0.041}_{-0.000}$
PTF09cnd	$0.162\ ^{+0.035}_{-0.019}$	$0.673\ ^{+0.100}_{-0.185}$
2010gx	$0.340\ ^{+0.015}_{-0.018}$	$0.349\ ^{+0.055}_{-0.046}$
PTF10hgi	$0.003\ ^{+0.008}_{-0.003}$	$0.351\ ^{+0.020}_{-0.016}$
SN2011ke	$0.177\ ^{+0.009}_{-0.007}$	$0.070\ ^{+0.016}_{-0.017}$
SN2011kf	$0.174\ ^{+0.061}_{-0.015}$	$0.124\ ^{+0.077}_{-0.090}$
PTF11dsf	$0.924\ ^{+1.849}_{-0.076}$	$2.651\ ^{+0.188}_{-1.368}$
PTF11rks	$0.602\ ^{+0.029}_{-0.000}$	$0.773\ ^{+0.080}_{-0.000}$
SN2012il	$0.212\ ^{+0.057}_{-0.009}$	$0.284\ ^{+0.177}_{-0.112}$

[a]Mass reported is an assumed fixed mass used within SED fitting.

In Fig. 5, we present the cumulative distribution of the absolute nIR magnitudes of the SLSNe hosts against those of the LGRBs and a subsample of GOODS CCSN hosts for which parallel photometric measurements were carried out. It can be seen here that SLSN hosts are in most cases much fainter than either LGRB hosts or CCSN hosts over the redshift range considered here. Breaking down by SLSN subtype, the most extreme examples (ignoring the small sample size of SLSNe-R) are the SLSN-I hosts, which are inconsistent with any other population of transient hosts. In contrast the SLSN-II hosts extend to magnitudes much fainter than CCSN host galaxies but at the brighter end of their distribution are comparable to the luminosities of LGRB hosts. In addition to the observed populations we also show as a solid cyan line the expected distribution of host magnitudes should they be drawn from the field population in proportion to the total nIR luminosity density (i.e. uniformly from the luminosity weighted luminosity function; Cirasuolo et al. 2007), demonstrating that all transient types arise from fainter galaxies than expected in this scenario. This is not surprising since weighting the luminosity function by the nIR is approximately equivalent to weighting by galaxy mass, and as such we see a significant contribution from massive, but largely quiescent galaxies which will not host core-collapse events.

Downloaded from http://mnras.oxfordjournals.org/ at California Institute of Technology on June 2, 2016

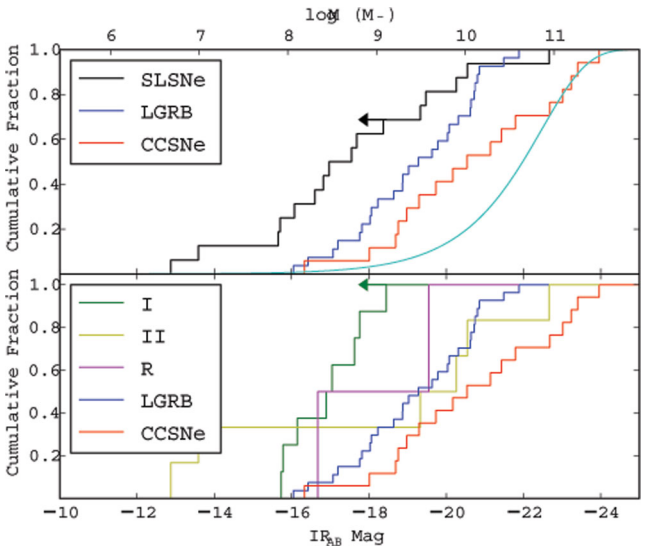

Figure 5. Upper panel: cumulative frequency distribution of the absolute nIR magnitudes of core-collapse event host galaxies. Arrows represent cases in which no host was detected and the 3σ limiting magnitude is used to place an upper limit upon the brightness of these hosts. The difference between the distributions of the SLSN and other core-collapse hosts is statistically significant, with probabilities of 0.008 and 0.0017 of the SLSN hosts being drawn from the same population as LGRB and CCSN hosts, respectively. We also display the nIR galaxy luminosity function for galaxies within our brightness range (cyan line; Cirasuolo et al. 2007). Using nIR brightness as a proxy for mass (top x-axis), we can expect our hosts to be significantly less massive too. Lower panel: we present the same distributions with the hosts of SLSNe broken down by classification. Here, the SLSN classes appear indistinguishable from one another in brightness, but this is likely due to small number statistics. We perform AD testing between the different subclasses and both core-collapse comparison groups, and find SLSN-I hosts to be inconsistent with our sample of core-collapse transients, although we find a stronger association for SLSN-II, due to the much broader distribution in brightness it exhibits.

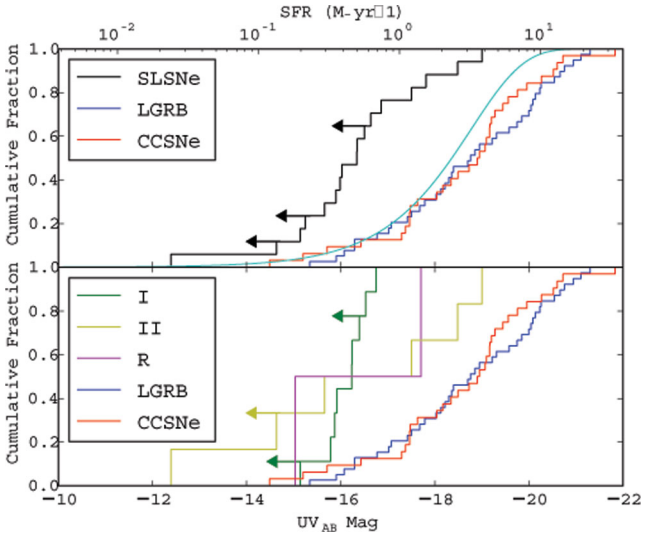

Figure 6. Cumulative distribution of the UV luminosities of SLSN, LGRB and CCSN host galaxies (upper panel). AD results show that SLSN hosts are not drawn from the same distribution of hosts at a high confidence ($p = 4.1 \times 10^{-5}$ and $p = 5.4 \times 10^{-5}$ for LGRBs and CCSNe, respectively). We also display the Baldry et al. (2005) UV galaxy luminosity function for galaxies within our brightness range (cyan line). Using UV brightness as a proxy for SFR (top x-axis), we can expect our hosts to be substantially less star forming than our comparison samples. Breaking this down by SLSN type (lower panel) shows little distinction between the subclasses, although again small number statistics are likely to be an influence here. AD testing between subclasses proves a strong inconsistency between the all classes of SLSN hosts and our comparison samples in $M_{\rm UV}$.

Fig. 6 shows the same analysis for the UV luminosity distribution of the SLSNe sample. Again, the SLSNe are markedly fainter (hence lower SFR) than the GRBs or CCSNe. However, since they are also faint in the nIR their inferred specific star formation rates (SFR/M), do not suggest that they are forming stars an a rate unusually low for their mass, and they would still class as actively star-forming galaxies. Interestingly in this UV range the CCSN and LGRB hosts appear to be more similar, although it should be noted that due to the paucity of UV observations of CCSNe in GOODS, this CCSNe host sample is different from the one used for our nIR comparison. The similarity of LGRB and CCSNe hosts in the UV, and the differences in the nIR could also be explained by the typically higher specific SFRs of GRB hosts (Castro Cerón et al. 2006; Svensson et al. 2010).

To formalize the significance of these differences we perform both Kolmogorov–Smirnov (KS) and Anderson–Darling (AD) tests of each population [including a separate tests for our SLSNe and combined (SLSNe+LSNe) samples]. The AD test provides a sample comparison more sensitive to the ends of the distribution, which in light of the extremely faint nature of some of our sample, may provide a more apt test statistic than the KS test. Hence we refer to the AD statistic throughout the rest of this work, although our conclusions would be unaffected by the use of the KS-test. The probabilities of an underlying association between different distributions are presented in Table 4, and the results indicate that the probability of the SLSN host sample and the hosts of LGRBs and CCSNe being drawn from the same pool of galaxies is low. As expected the differentiation is strongest for the SLSN-I hosts, which reject the hypothesis that they arise from hosts with similar absolute magnitudes to either CCSN or GRB host galaxies, in both cases indicating that the host galaxies are significantly less luminous, with further implications for their masses and SFRs (see below).

The SLSN-II hosts have low to modest probabilities of being drawn from the same underlying host population as both the LGRBs ($P = 0.01$, 0.23 for UV and nIR, respectively) and the CCSNe ($P = 0.008$, 0.29 for UV and nIR). However, as previously noted the most striking feature of the SLSN-II hosts is their presence over a wide range of luminosity from our brightest host (SN 2006gy, $M_{\rm nIR} \sim -22.5$) to our faintest two (SN 2008es, SN 2008fz, $M_{\rm nIR} \sim -13$). Should these galaxies be drawn from some star formation (or mass) weighted distribution, the chance of obtaining any such faint hosts within a small sample would be very small. For example, the expected number based on the extrapolation of a luminosity function is $\ll 1$. Indeed, KS and AD tests suffer from a lack of sensitivity to such extremes since they measure the maximum offset between two distributions, and are insensitive to these extremes. Despite the small number statistics, the presence of two SLSNe-II in such faint host suggests than unusual mechanisms may be at play in at least some of these events.

We present our SED fits to all our targets in Fig. 7, and our derived properties in Table 3. We compare these stellar masses and SFRs to those found through proxies from our nIR and UV luminosities, which provides a model independent check upon our SED fit values, and find them to be generally of the same order of magnitude. Using the properties derived from the SED fitting, we present the distribution of masses and SFRs for our sample in Figs 8 and 9, respectively, alongside those properties which have been derived

Downloaded from http://mnras.oxfordjournals.org/ at California Institute of Technology on June 2, 2016

Table 4. Two sample AD probability results between samples. Probabilities $<\sim \times 10^{-6}$ are given 0.0.

		SLSNe sample		Combined sample[a]	
Data set	Host connection connection	KS stat.	AD stat.	KS stat.	AD stat.
	SLSNe–LGRB	0.013	0.008	0.022	0.020
nIR Magnitude	SLSNe–CCSNe	0.005	0.0017	0.009	0.003
	SLSNe-I–LGRB	8.1×10^{-4}	8.1×10^{-5}	$1.5x10^{-4}$	8.7×10^{-5}
	SLSNe-I–CCSNe	1.5×10^{-5}	6.8×10^{-5}	4.4×10^{-5}	6.8×10^{-5}
	SLSNe-II–LGRB	0.55	0.23	0.77	0.33
	SLSNe-II–CCSNe	0.61	0.29	0.56	0.27
	LGRB–CCSNe	0.05	0.04	–	–
	SLSNe–LGRBs	1.0×10^{-4}	4.1×10^{-5}	4.1×10^{-5}	3.7×10^{-5}
UV Magnitude	SLSNe–CCSNe	1.4×10^{-5}	5.4×10^{-5}	4.9×10^{-6}	6.5×10^{-5}
	SLSNe-I–LGRB	2.4×10^{-6}	2.7×10^{-5}	2.5×10^{-6}	1.9×10^{-5}
	SLSNe-I–CCSNe	1.7×10^{-6}	5.0×10^{-5}	0.0	2.7×10^{-5}
	SLSNe-II–LGRB	0.13	0.01	0.04	0.005
	SLSNe-II–CCSNe	0.06	0.008	0.053	0.011
	LGRB–CCSNe	0.85	0.80	–	–
	SLSNe–LGRB	0.0	0.07	0.0	0.14
Masses	SLSNe–CCSNe	0.0	0.007	0.0	0.007
	SLSNe-I–LGRB	0.002	1.2×10^{-5}	8.6×10^{-4}	0.0
	SLSNe-I–CCSNe	8.9×10^{-5}	0.0	2.6×10^{-5}	0.0
	SLSNe-II–LGRB	0.65	3.3×10^{-5}	0.92	1.6×10^{-5}
	SLSNe-II-CCSNe	0.49	1.32×10^{-5}	0.78	0.0
	LGRB–CCSNe	0.48	0.12	–	–
	SLSNe–LGRB	6.2×10^{-5}	7.7×10^{-5}	3.5×10^{-5}	8.4×10^{-5}
SFRs	SLSNe–CCSNe	0.0	0.0	0.0	0.0
	SLSNe-I–LGRB	8.2×10^{-5}	3.0×10^{-4}	9.0×10^{-5}	1.7×10^{-4}
	SLSNe-I–CCSNe	0.0	1.34×10^{-5}	0.0	1.1×10^{-5}
	SLSNe-II–LGRB	0.016	0.065	0.09	0.02
	SLSNe-II–CCSNe	0.016	0.0013	0.04	0.002
	LGRB–CCSNe	0.11	0.06	–	–
r_{80}	SLSNe–LGRB	0.0	1.0×10^{-5}	0.0	1.5×10^{-5}
	SLSNe–CCSNe	1.4×10^{-4}	1.1×10^{-4}	7.3×10^{-4}	3.6×10^{-4}
	LGRB–CCSNe	0.15	0.09	–	–

[a]Excluding SN 1997cy.

from SED fitting for LGRB and CCSN hosts from Fruchter et al. (2006) and Svensson et al. (2010). As suggested by proxies, we can see that SLSN hosts are less massive and possess lower SFRs than CCSN and LGRB hosts, to a high level of significance, as show in Table 4.

A comparison of the measured r_{80} values from our nIR observations is presented in Fig. 10, combined with the masses to provide an indication of the relative evolution of size with luminosity for our core-collapse transient host sample. The compact and low-mass nature of the SLSN hosts is clearly visible, as they occupy a distinct region of parameter space from other core-collapse hosts of similar brightness. We note that CCSN hosts are in turn more compact than SDSS galaxies (e.g. Kelly et al. 2010), whose size distribution peaks well above of the range of sizes presented within this work. Again, AD tests between the *HST* SLSNe and comparison samples give little probability that they are drawn from the same underlying population. It should be noted that our nIR observations are frequently rather short, and so low surface brightness features could be missed in comparison to deeper observations of the GRB hosts and GOODS SNe. However, we evaluate the probability of this using modelling of galaxies to estimate our expected recovery rate. We find that even if SLSN hosts were to lie at the extrema of their error bars (i.e. if there were a systematic shift of each point by 1σ larger) the result would still be statistically significant to 1×10^{-4} and 0.014 for LGRBs and CCSNe, respectively.

Given that the redshift distributions of these classes of transient exhibit somewhat different functional forms it is reasonable to ask if the observed differences in the properties of the population are due to redshift evolution in the host galaxies, rather than the properties of the progenitor stars themselves.

Ideally it may be beneficial to conduct tests considering only low-z SLSNe (e.g. $z < 0.4$) and with comparison samples at the same redshift. However, our comparison samples become very small at these low-redshifts, frequently with <4–8 objects for comparison (see Fig. 1). For these small sample sizes we lack the statistical power to make strong statements about redshift evolution within the SLSNe sample in comparison to those of others. Given that there is some evidence for evolution in LGRB properties with redshift, albeit occurring predominantly around $z \sim 1$ (Perley et al. 2016) it is possible that some apparent differences between SLSNe and other transient populations are amplified, or damped, by evolution in the host properties themselves.

We also determine specific SFRs (sSFRs) for our SLSN hosts, which we present within Fig. 11. When compared alongside those of LGRBs and CCSNe from Svensson et al. (2010), appear to fall within a similar range of sSFR as other core-collapse transients. Although, when compared to a wider sample of galaxies, as carried

Downloaded from http://mnras.oxfordjournals.org/ at California Institute of Technology on June 2, 2016

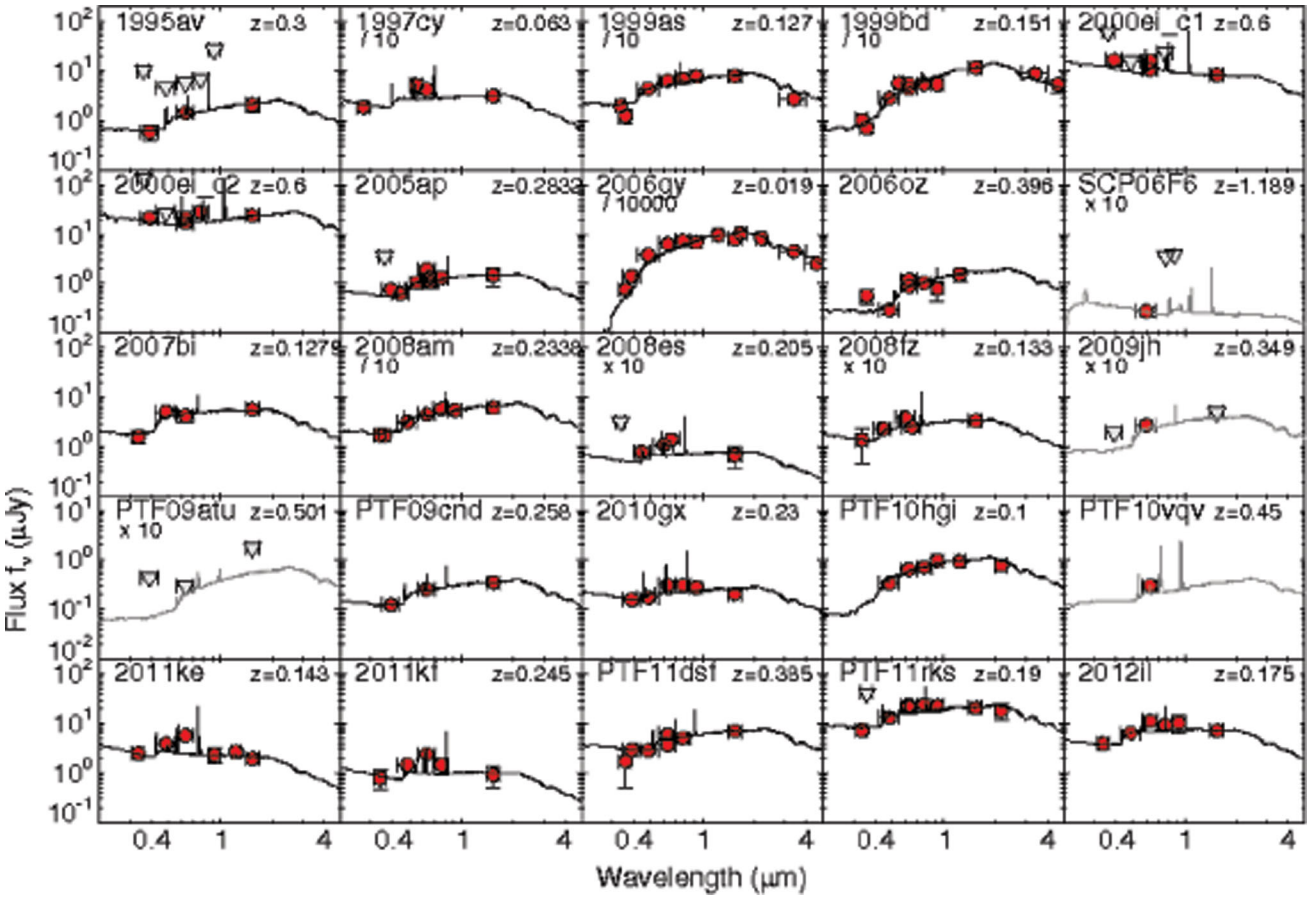

Figure 7. SED fits of SLSN hosts as carried out in a similar manner to Perley et al. (2013), using photometric results from our *HST* programmes and WHT and VLT images, in addition to results from literature and SDSS. Arrows indicate upper limits to photometry

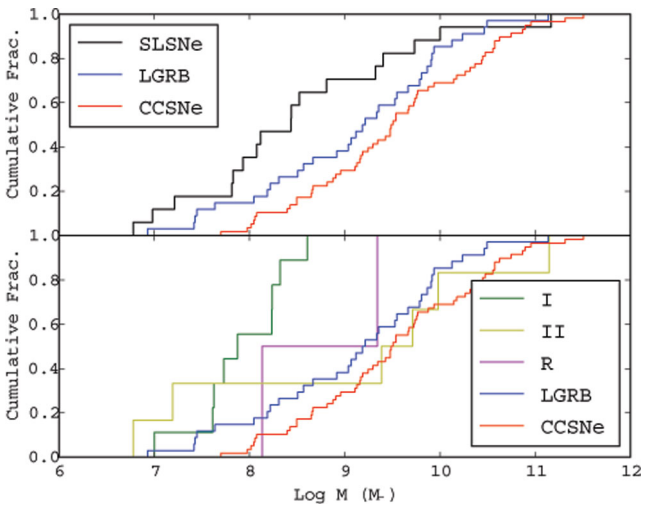

Figure 8. Masses of transient hosts as determined by SED fits. SLSN hosts are significantly less massive than CCSNe host galaxies, and show a 1σ difference to LGRB hosts. Splitting by subtype, we again find little similarity between the subclasses of SLSN hosts and our comparison samples

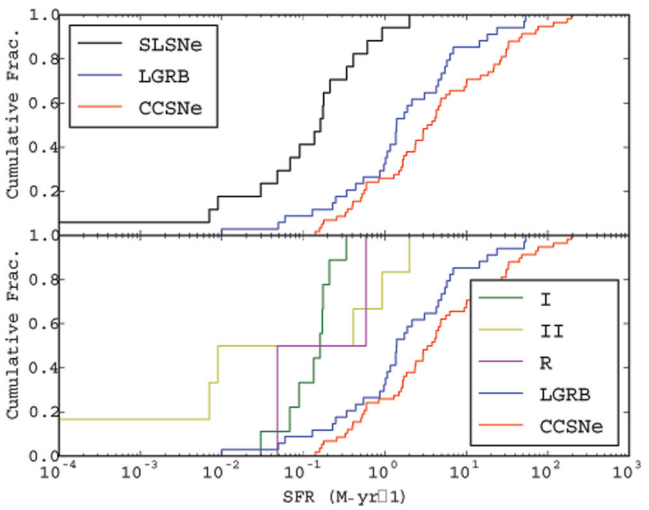

Figure 9. SFR for transient hosts determined by SED fitting. SLSN hosts are seen to be not as strongly star forming as CCSNe or LGRB host galaxies, with very low probabilities of the distributions being from the same underlying population. Again, splitting by subtype shows little deviation from this result for the hosts of SLSNe-I, however for those of SLSNe-II, there appears to be slight overlap between it and the LGRB hosts distribution ($p = 0.065$). However, the evolution exhibited within the average SFR of LGRB hosts over low redshift (Perley et al. 2013, 2016; Schulze et al. 2015) may somewhat bias our results.

out by Castro Cerón et al. (2006, ref. their fig. 2) and Svensson et al. (2010, ref. their fig. 7), such as distant red galaxies (DRGs), submillimeter galaxies (SMGs) and Lyman break galaxies (LBGs), the sSFRs of the core-collapse transients lie at lower masses for a given sSFR than DRGs, SMGs and LBGs.

Downloaded from http://mnras.oxfordjournals.org/ at California Institute of Technology on June 2, 2016

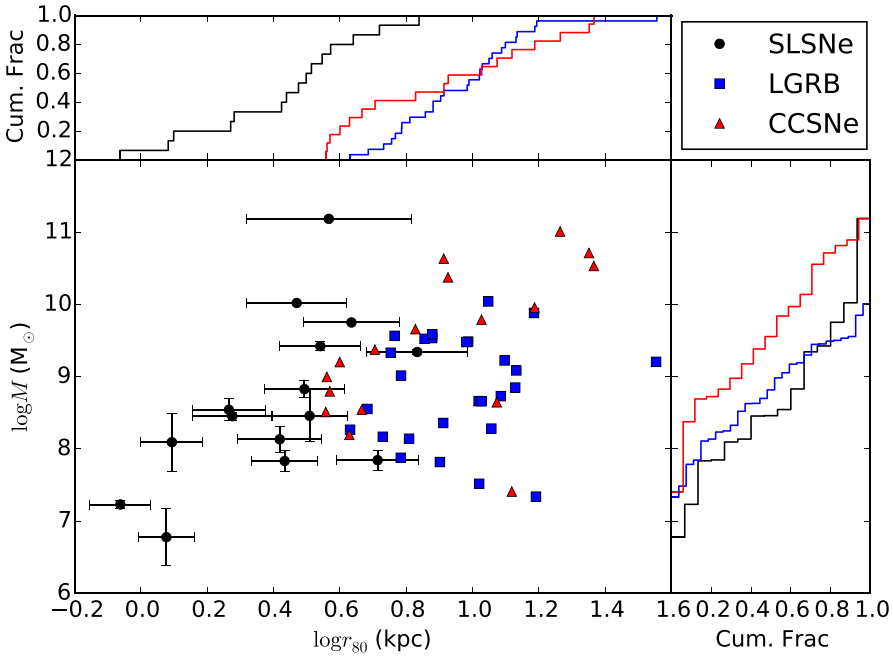

Figure 10. r_{80} light profiles measured in the *HST F*160*W* band of core-collapse hosts against their mass as derived from SED fitting. Error bars are indicative of SEXTRACTORS ability to detect the edge of a galaxy at given brightness for a given redshift. The compact nature of SLSN hosts is apparent here.

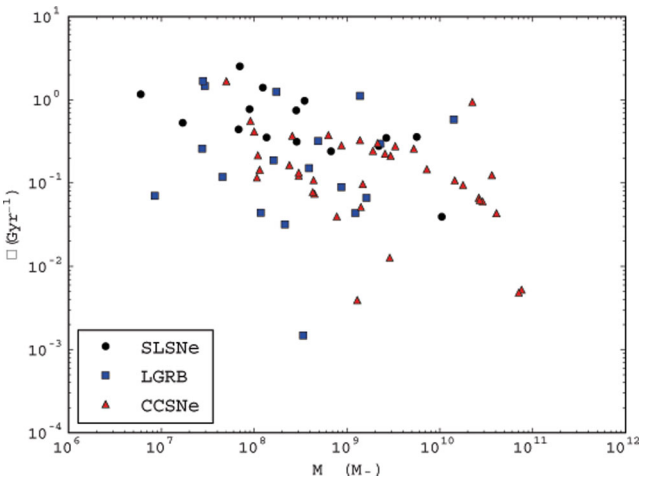

Figure 11. sSFR values for SLSN, CCSN and LGRB hosts against their respective stellar masses. Overall, the hosts of SLSNe appear to occupy a similar range of sSFR values as CCSN and LGRB host galaxies. Note we do not include the host of SN 2006gy here, due to its poorly constrained SFR from SED fitting.

6 DISCUSSION

The observations presented within this work highlight the extreme nature of the SLSN host population. A significant fraction arise in galaxies of exceptionally low luminosity, both in the UV and nIR. These galaxies are extreme even when compared to other populations of core-collapse hosts, or even to GRBs, whose host galaxies are already set well apart from a typical field sample. Given that the UV and IR naturally provide a probe of both star formation and stellar mass, these differences are indicative of extremely low-mass star-forming hosts for SLSNe. Indeed, studies of SDSS galaxies indicate that there is little contribution to the global SFR in the local Universe from galaxies with $M_{UV} > -17$ (Blanton et al. 2005; Graham & Fruchter 2013), where we have shown the majority of the SLSN hosts within our sample lie, as can be seen in Fig. 6. This result also holds in comparison to the host galaxies of CCSNe and LGRBs, the latter of which have been suggested to arise predominantly, if not exclusively from stars of low to moderate metallicity (e.g. Fruchter et al. 2006; Graham & Fruchter 2013; Perley et al. 2015). The host galaxies are also typically small, but exhibit surface star formation densities, and specific SFRs that are more in keeping with those of other transient populations (i.e. they lie at the low end of most physical parameters compared to other core-collapse transient hosts, such that any additional parameter derived with reference to two or more of SFR, mass and size, does not provide a strong distinction between the hosts of SLSNe and other star-forming galaxies). The majority of our hosts exhibit high star formation surface densities, higher than those seen in the hosts of SNe-Ib/c and SNe-II, more akin to broad line SN-Ic and GRB hosts (Kelly et al. 2014), in agreement with the results of Lunnan et al. (2015).

However, these broad conclusions based on all SLSNe fail to consider the diversity of SLSN types. In splitting the sample by type (utilizing the classification system of Gal-Yam 2012), small number statistics prevent us from drawing strong conclusions about differences *between* SLSN subtypes, although it does appear that SLSNe-I arise from predominantly fainter host galaxies than SLSNe-II on average. The larger differences between SLSNe and other classes of transient (compared to the differences between classes of SLSNe), do allow us to draw stronger conclusions when comparing the host galaxies of SLSNe-I and SLSNe-II to the hosts of LGRBs and CCSNe.

The SLSN-I hosts are much fainter than the hosts of either CCSNe or LGRBs. Since the LGRBs are frequently explained as arising from low metallicity systems, the logical conclusion might

Downloaded from http://mnras.oxfordjournals.org/ at California Institute of Technology on June 2, 2016

be to assign SLSNe-I to progenitors of even lower metallicity. This however is problematic; spectroscopic observations of the hosts of SLSNe (Lunnan et al. 2014; Leloudas et al. 2015) generally show modest metallicities, and indeed Lunnan et al. (2014) conclude the metallicities of SLSNe-I are consistent with those of GRB hosts. There are multiple possible origins for this discrepancy.

First, it may be that rapid evolution in the properties of LGRBs hosts with redshift magnifies what is in fact a small difference between the metallicity cuts for SLSNe and LGRBs. Although small sample sizes prevent us from testing this reliably, it is not unlikely that evolution within the LGRB host population below $z \sim 1$ may accentuate the apparent differences between themselves and SLSN hosts. Additionally, the samples utilized by Lunnan et al. (2014), Leloudas et al. (2015) and this work, while containing some overlap are also significantly different. Small number statistics may then represent a potential concern.

Selection effects could also hinder such work. For example, many SLSNe have been found by searches targeting orphan transients (those without visible hosts in the survey images), since the SLSNe so effectively outshines it host galaxy. This may immediately remove SLSNe in higher metallicity, more luminous hosts, causing the remaining sample to be biased towards a lower metallicity. We can attempt to address this by adopting the Pan-STARRS limiting magnitude cut of $R \sim 23.5$ for host galaxy detection across all of our host samples (SLSNe, CCSNe and GRBs), such that we include *only* hosts fainter than this limit (we note that this is the most conservative approach since the limiting magnitudes of the other surveys finding SLSNe are typically significantly brighter). We recover 8/21 hosts from our *HST* SLSN sample using this approach. Within this limit the SLSN host sample appears fainter and less massive than the CCSNe and LGRB host samples. Although here we are once again dominated by small number statistics within our comparison hosts it suggests that the differences between the differing populations are not created by the selection mechanisms of the transient surveys. The impact of the faintest galaxies may operate in the opposite direction, very faint galaxies are difficult to obtain metallicities for, and so if these are omitted it may bias the observed metallicity distribution towards higher levels.

Finally, it is relevant to consider if astrophysical effects could be at play. Mass (or luminosity)–metallicity relations have been used to infer the metallicities of GRB host galaxies, and this could be extended to SLSN hosts. In this case one might infer a metallicity threshold based on the most luminous observed SLSN host galaxy, and could then test the consistency of the distribution of fainter (and using an L–Z relation, lower metallicity) galaxies. In this case the observed distribution of SLSNe-I would be broadly in keeping with expectations. For the UV luminosity function of Baldry et al. (2005), truncated at $M_{\rm UV} \sim -16.8$ (our most luminous SLSN-I host) we would expect ∼60 per cent of the UV-light (hence SFR, or equivalent number of SNe) to arise from galaxies within one-magnitude of this luminosity. This would match well the relatively narrow range of luminosities observed for the host galaxies of SLSNe-I, while the two upper limits (of nine SNe) are consistent with the fainter fraction of the hosts. To this end, metallicity may appear an good description of the observed luminosity distribution. However, it is clear such relations between luminosity or mass and metallicity are crude at best; often GRB hosts are found to have low metallicity, even when in relatively luminous hosts (see e.g. fig. 10 in Graham & Fruchter 2013). If SLSN hosts lie systematically low in metallicity when compared to mass in the mass–metallicity relationship then it would not be surprising that they could appear very different from LGRBs in mass, but rather more similar in metallicity. It is also possible that an apparent discrepancy in interpretation may arise due to the different locations of SLSNe and GRBs on their host galaxy light distributions. GRBs are preferentially concentrated on the brightest regions of their host galaxies. In these situations the global metallicity of the host galaxy (which comes from 'most' of the light) might be a reasonable proxy for the metallicity in the GRB region (although see e.g. Hammer et al. 2006 for some caveats). In the case of SLSNe, the concentration is not so strong (Lunnan et al. 2015), and indeed some events (e.g. SN2009jh) lie apparently off their host galaxy light. In these scenarios it is more likely that the global host metallicity is not indicative of the metallicity at the location of the SNe, and so spatially resolved measurements are urgently needed.

Theoretically, there are good reasons to favour similarities between the environments of LGRBs and SLSNe-I. It is known that LGRBs arise from central engines (Woosley 1993), and there is growing consensus that this is also the case for SLSNe-I (Kasen & Bildsten 2010; Dexter & Kasen 2013), which become active during the collapse of very massive stars. Observations of both classes of event provide evidence favouring this model (for SLSNe Levan et al. 2013; Nicholl et al. 2013, 2015; for LGRBs e.g. Metzger et al. 2011, although for association with luminous SNe; see Mazzali et al. 2014). If this is the case then we might expect the production of these engines to be favoured in similar environments. However, there are differences in the necessary engine properties to create LGRBs or SLSNe. In particular, in LGRBs, the bulk of the energy must be released extremely early ($\sim 10^3$ s) to power the ultrarelativistic outflow, this energy is then deposited into the ejecta close to the engine. In contrast, for SLSNe the engine must act to re-engerize the outflow on time-scales of weeks to months after the initial core collapse. In the case of black hole engines this means the accretion time-scales must vary by many orders of magnitude, while for magnetars the crucial spin-down parameter must also be different.

Relative numbers of magnetars observed within the Milky Way, when placed in context with the galactic CCSN rate, requires that ∼10 per cent of these events result in the birth of a magnetar (Mereghetti, Pons & Melatos 2015). This rate is far higher than any suggested for SLSNe and suggests that the magnetars we observe in the Galaxy today have little connection to those that may be created in luminous SNe explosions. Rotation is a logical difference between those systems creating 'normal' magnetars, and those which are powerful enough to re-energize explosions, and this may in turn provide an natural explanation for environmental biases. At higher metallicities the line driven winds will dramatically brake the rotation of the star prior to a SN explosion, and hence conservation of magnetic flux and angular momentum upon core collapse may create a magnetar with a longer rotation period than needed to explain either GRBs or SLSNe. Hence we might expect to observe both LGRBs and SLSNe in relatively metal poor environments. Indeed, since the spin periods for the GRB magnetars are shorter than for those creating SLSNe (or they have higher magnetic fields) one might naively assume that GRBs could favour even lower metallicity. In this regard it is valuable to note the recent example of GRB 111209A, an ultralong GRB in a low metallicity galaxy (Levan et al. 2014a) in which a magnetar may have produced both the GRB and luminous SNe (Greiner et al. 2015).

We have only two SLSNe-R within our sample, and so can say little about the properties of their hosts in comparison to other samples, aside from noting that their luminosity is generally in keeping with those of SLSNe-I, which some authors have suggested is their correct assignment. We do note that interestingly in both cases the

Downloaded from http://mnras.oxfordjournals.org/ at California Institute of Technology on June 2, 2016

SLSNe-R appear to originate from bright UV regions within their hosts, something that is not the case for all SLSNe-I, but given the small sample size and available data it is not possible to investigate if they may arise from young, massive stellar populations in metal poor regions, more so than the environments of SLSNe-I. It is also relevant to note that recent calculations suggest that stars at modest metallicity and mass can create pair instability SNe (Yusof et al. 2013) and so the environment alone may not ultimately provide as strong a means of discrimination between models as had previously been hoped.

Less attention has been paid to the host galaxies of SLSNe-II, partly as the interaction model for their origin appears a more natural explanation given the likely presence of recently ejected hydrogen envelopes in Type-IIn SNe (and most SLSNe-II are of the IIn variety). However, their hosts span a very wide range of luminosity, including two host galaxies that are fainter than any SLSNe-I, LGRB or CCSN host in our sample. Indeed, while a handful of SNe Ia have been found in comparably faint systems (e.g. Strolger et al. 2002) the presence of any type of core-collapse SNe in galaxies fainter than $M_B \sim -14$ is extremely rare (for example, none in the cross-correlation of the SAI catalogue with SDSS; Prieto, Stanek & Beacom 2008). Although this may in part be due to a lack of follow-up, in practice at these modest redshifts essentially no SNe would be expected, even with the metallicity cuts used to explain the GRB population (Graham & Fruchter 2013). The presence of two host galaxies in such low luminosity galaxies is then puzzling; whatever mechanism is at play must be able to produce SNe across this wide range of galaxy types. Metallicity dependence here seems a less likely scenario, unless those SLSNe-II apparently born in the most luminous hosts are in fact born in lower mass dwarf galaxies within their haloes (although in this case it would be odd that some SLSNe-I were not also seen in similar environments). However, other possible mechanisms may provide a viable alternative. For example, if SLSNe-II were formed only from very massive stars then they may exist only in very special locations. If the core mass prior to SN is the dominant factor then indeed low metallicity will preserve core masses much better than at higher metallicity due to far lower radiative mass-loss rates, and a possible bias to a more top heavy initial mass function at lower metallicity. However, if SLSNe-II are in fact best explained by a strong interaction model then large scale mass-loss is necessary at some point. In this case, the conditions necessary to form a SLSNe-II may be a combination of both relatively high core mass and still significant mass-loss, meaning the initial (i.e. total) mass could play a more important role. In this regard it is interesting to note that the formation of very massive stars is potentially affected by stochastic processes even without changes in metallicity or to the underlying IMF. Small star-forming regions, following a typical initial mass function, have a lower probability of building most massive stars, because there is insufficient mass. For example, if a star-forming region will form only a few hundred solar masses of stars the probability of it forming any stars with greater than $\sim$100 $M_\odot$ is extremely small, stochastic sampling assumes that masses are picked at random from the IMF, but that the star can only be formed should sufficient mass remain in the cluster. Hence, once a few stars have been formed, forming extremely massive stars in low-mass clusters becomes unlikely. Stochastic sampling effects have been observed in relatively local open clusters, and appear to be very important below cluster masses of $\sim 10^4$ $M_\odot$ (Piskunov et al. 2009). Indeed, the most massive star in a cluster is thought to scale roughly as $0.39 M_{\rm cluster}{}^{2/3}$ (Bonnell et al. 2001; Weidner, Kroupa & Bonnell 2010), meaning that clusters with initial masses of $\sim 10^4$ $M_\odot$ are needed to form stars with masses >200 $M_\odot$. The most massive stars would then be formed in locations where either there was a large-scale starburst (e.g. the very massive stars located in 30 Dor, or at a handful of locations within the Milky Way (Rauw & De Becker 2004; De Becker et al. 2006; Crowther et al. 2010; Gvaramadze et al. 2013; Hainich et al. 2014)), or in places where the IMF was biased towards the creation of high-mass stars (i.e. was top heavy relative to the local IMF). Indeed, it is interesting to note that the relative number of high-mass clusters (scaled by SFR) does appear to be higher in dwarf galaxies, or in starbursts (e.g. Bastian 2008), such that massive clusters, and hence the most massive stars may be found in relatively greater numbers in these galaxies, compared to relatively quiescent spirals such as the Milky Way. Qualitatively this model may have some appeal in explaining the unexpectedly large range of properties in the SLSN-II host population, although the lack of knowledge about variations in the IMF, even in the relatively local Universe precludes more detailed work. Finally, it is also possible that multiple progenitor routes are at play in the creation of the SLSNe-II population, meaning that some exhibit strong metallicity biases while others are formed at more typical metallicities, perhaps via binary interactions which may eject large mass reservoirs quickly during common envelopes etc.

7 SUMMARY

We have utilized the unparalleled UV and nIR sensitivity of *HST* to provide rest-frame UV and nIR observations of a sample of SLSNe. We find that the hosts of SLSNe-I are consistently fainter than other core-collapse hosts (CCSNe and LGRBs), by extension this should be indicative of a low-mass, SFR and metallicity. This is despite apparently similar metallicities observed between LGRBs and SLSNe-I from optical spectroscopy of SLSN hosts (including some hosts for which nIR and UV observations are presented here; Lunnan et al. 2014). This discrepancy may be explained by a combination of small sample sizes and the absence of the faintest host galaxies from spectroscopic samples, although despite the similarities in the favoured progenitors for LGRBs and SLSNe-I there are also good astrophysical motivations (for example the time-scales required in energy breakout and potentially the spin-down rate of any magnetar driven engines) as to why their environments may not be identical.

We find that SLSNe-II arise from galaxies spanning a surprisingly large range in absolute magnitude (and hence in SFR and stellar mass). This is difficult to explain from sampling the underlying star-forming galaxy population subject to a simple metallicity bias, as has been attempted for LGRBs and SLSNe-I, but may be due to the preferential production of very massive stars in certain environments (either massive star formation regions, or at low metallicity). Equally, it could be a reflection that the current classification system has failed to adequately capture the true diversity of progenitor routes for SLSNe-II.

Nevertheless it is clear that studies of SLSNe environments may still offer a powerful route to clues to their progenitor characteristics, in much the same way as they have for other classes of astrophysical transients. Such work will rely on a continuing stream of these very rare events, coupled with detailed follow-up across the electromagnetic spectrum. Through this detailed study of the environments we may hope to elucidate the progenitors of SLSNe, and how they fit in to the growing diversity now being discovered in the transient optical sky.

Downloaded from http://mnras.oxfordjournals.org/ at California Institute of Technology on June 2, 2016

ACKNOWLEDGEMENTS

CRA acknowledges receipt of a studentship from the Midlands Physics Alliance. AJL thanks STFC for support under grant ID ST/I001719/1, and the Leverhulme Trust for support via a Philip Leverhulme Prize. We are grateful to the PTF group (in particular Robert Quimby and Avishay Gal-Yam) for providing six images for SNe for astrometric purposes. ALJ, JDL and ERS are grateful for the support of STFC Warwick Astrophysics consolidated grant ID ST/L000733/1. Based on observations made with the NASA/ESA *HST*, obtained at the STScI, which is operated by the Association of Universities for Research in Astronomy, Inc., under NASA contract NAS 5-26555. These observations are associated with program GO-13025 and GO-13480. Based on observations made with ESO Telescopes at the La Silla Paranal Observatory under programme ID 092.D-0815. Optical data were obtained from the WHT under service mode programme SW2012b31.

REFERENCES

Abazajian K. N. et al., 2009, ApJS, 182, 543
Ahn C. P. et al., 2012, ApJS, 203, 21
Anderson J., Bedin L. R., 2010, PASP, 122, 1035
Anderson J. P., Habergham S. M., James P. A., Hamuy M., 2012, MNRAS, 424, 1372
Appenzeller I. et al., 1998, The messenger, 94, 1
Baldry I. K. et al., 2005, MNRAS, 358, 441
Barbary K. et al., 2009, ApJ, 690, 1358
Bastian N., 2008, MNRAS, 390, 759
Bertin E., Arnouts S., 1996, A&AS, 117, 393
Blanton M. R., Lupton R. H., Schlegel D. J., Strauss M. A., Brinkmann J., Fukugita M., Loveday J., 2005, ApJ, 631, 208
Bloom J. S., Kulkarni S. R., Djorgovski S. G., 2002, AJ, 123, 1111
Bloom J. S. et al., 2009, ApJ, 691, 723
Bonnell I. A., Clarke C. J., Bate M. R., Pringle J. E., 2001, MNRAS, 324, 573
Bourque M. et al., 2013, American Astronomical Society Meeting Abstracts, Vol. 222, p. 316.11
Cano Z., 2013, MNRAS, 434, 1098
Castro Cerón J. M., Michałowski M. J., Hjorth J., Watson D., Fynbo J. P. U., Gorosabel J., 2006, ApJ, 653, L85
Chatzopoulos E. et al., 2011, ApJ, 729, 143
Chen T. W. et al., 2015, MNRAS, 452, 1567
Chevalier R. A., Irwin C. M., 2011, ApJ, 729, L6
Cirasuolo M. et al., 2007, MNRAS, 380, 585
Cooke J. et al., 2012, Nature, 491, 228
Cool R. J. et al., 2007, GCN Circ., 6510, 1
Crowther P. A., Schnurr O., Hirschi R., Yusof N., Parker R. J., Goodwin S. P., Kassim H. A., 2010, MNRAS, 408, 731
Dahlen T. et al., 2003, BAAS, 35, 1278
Davies B., Figer D. F., Kudritzki R.-P., Trombley C., Kouveliotou C., Wachter S., 2009, ApJ, 707, 844
De Becker M., Rauw G., Manfroid J., Eenens P., 2006, A&A, 456, 1121
Dexter J., Kasen D., 2013, ApJ, 772, 30
Drake A. J. et al., 2009, ApJ, 696, 870
Drake A. J. et al., 2010, ApJ, 718, L127
Dressel L., 2012, Wide Field Camera 3 Instrument Handbook for Cycle 21 v. 5.0.
Drout M. R. et al., 2011, ApJ, 741, 97
Eldridge J. J., Izzard R. G., Tout C. A., 2008, MNRAS, 384, 1109
Elliott J. et al., 2013, A&A, 556, A23
Fox O. D. et al., 2015, MNRAS, 454, 4366
Fruchter A. S., Hook R. N., 2002, PASP, 114, 144
Fruchter A. S. et al., 2006, Nature, 441, 463
Fynbo J. P. U. et al., 2009, ApJS, 185, 526
Gal-Yam A., 2012, Science, 337, 927
Gal-Yam A. et al., 2009, Nature, 462, 624
Gänsicke B. T., Levan A. J., Marsh T. R., Wheatley P. J., 2009, ApJ, 697, L129
Germany L. M., Reiss D. J., Sadler E. M., Schmidt B. P., Stubbs C. W., 2000, ApJ, 533, 320
Gezari S. et al., 2009, ApJ, 690, 1313
Graham J. F., Fruchter A. S., 2013, ApJ, 774, 119
Greiner J. et al., 2015, Nature, 523, 189
Gvaramadze V. V., Kniazev A. Y., Chené A.-N., Schnurr O., 2013, MNRAS, 430
Hainich R. et al., 2014, A&A, 565, A27
Hammer F., Flores H., Schaerer D., Dessauges-Zavadsky M., Le Floc'h E., Puech M., 2006, A&A, 454, 103
Hamuy M. et al., 2003, Nature, 424, 651
Harris W. E., 1996, AJ, 112, 1487
Heger A., Woosley S. E., 2002, ApJ, 567, 532
Hjorth J. et al., 2012, ApJ, 756, 187
Holland S. T. et al., 2010, ApJ, 717, 223
Howell D. A. et al., 2013, ApJ, 779, 98
Hudelot P. et al., 2012, VizieR Online Data Catalog, 2317, 0
Inserra C., Smartt S. J., 2014, ApJ, 796, 87
Inserra C. et al., 2013, ApJ, 770, 128
Jakobsson P. et al., 2006, A&A, 447, 897
James P. A., Anderson J. P., 2006, A&A, 453, 57
Kaiser N., Pan-STARRS Team, 2005, BAAS, 37, 150.04
Kasen D., Bildsten L., 2010, ApJ, 717, 245
Kelly P. L., Kirshner R. P., Pahre M., 2008, ApJ, 687, 1201
Kelly P. L., Hicken M., Burke D. L., Mandel K. S., Kirshner R. P., 2010, ApJ, 715, 743
Kelly P. L., Filippenko A. V., Modjaz M., Kocevski D., 2014, ApJ, 789, 23
Kennicutt R. C., Jr, 1998, ARA&A, 36, 189
Knop R. et al., 1999, IAU Circ., 7128, 1
Kochanek C. S., 2014, ApJ, 785, 28
Krühler T. et al., 2011, A&A, 534, A108
Larson D. et al., 2011, ApJS, 192, 16
Larsson J., Levan A. J., Davies M. B., Fruchter A. S., 2007, MNRAS, 376, 1285
Law N. M., Kulkarni S., Ofek E., Quimby R., Kasliwal M., Palomar Transient Factory Collaboration, 2009, BAAS, 41, 469.01
Leloudas G. et al., 2012, A&A, 541, A129
Leloudas G. et al., 2015, MNRAS, 449, 917
Lennarz D., Altmann D., Wiebusch C., 2012, A&A, 538, A120
Levan A. J. et al., 2007, MNRAS, 378, 1439
Levan A. J., Read A. M., Metzger B. D., Wheatley P. J., Tanvir N. R., 2013, ApJ, 771, 136
Levan A. J. et al., 2014a, ApJ, 781, 13
Levan A. J. et al., 2014b, ApJ, 792, 115
Lunnan R. et al., 2014, ApJ, 787, 138
Lunnan R. et al., 2015, ApJ, 804, 90
Lyman J., Bersier D., James P., Mazzali P., Eldridge J., Fraser M., Pian E., 2016, MNRAS, 457, 328
McConnachie A. W., 2012, AJ, 144, 4
McBreen S. et al., 2010, A&A, 516, A71
Mazzali P. A., McFadyen A. I., Woosley S. E., Pian E., Tanaka M., 2014, MNRAS, 443, 67
Mereghetti S., Pons J. A., Melatos A., 2015, Space Sci. Rev., 191, 315
Metzger B. D., Giannios D., Thompson T. A., Bucciantini N., Quataert E., 2011, MNRAS, 413, 2031
Miller A. A. et al., 2009, ApJ, 690, 1303
Miller A. A., Smith N., Li W., Bloom J. S., Chornock R., Filippenko A. V., Prochaska J. X., 2010, AJ, 139, 2218
Modjaz M. et al., 2008, AJ, 135, 1136
Neill J. D. et al., 2011, ApJ, 727, 15
Nicholl M. et al., 2013, Nature, 502, 346
Nicholl M. et al., 2015, ApJ, 807, L18
Ofek E. O. et al., 2007, ApJ, 659, L13

Downloaded from http://mnras.oxfordjournals.org/ at California Institute of Technology on June 2, 2016

Oke J. B. et al., 1995, PASP, 107, 375
Pérez-Ramírez D. et al., 2013, in Castro-Tirado A. J., Gorosabel J., Park I. H., eds, Gamma-ray Bursts: 15 Years of GRB Afterglows. EAS Publ. Ser. Vol. 61, p. 345
Perley D. A. et al., 2013, ApJ, 778, 128
Perley D. A. et al., 2015, ApJ, 801, 102
Perley D. A. et al., 2016, ApJ, 817, 8
Piskunov A. E., Kharchenko N. V., Schilbach E., Röser S., Scholz R.-D., Zinnecker H., 2009, A&A, 507, L5
Podsiadlowski P., Joss P. C., Hsu J. J. L., 1992, ApJ, 391, 246
Prieto J. L., Stanek K. Z., Beacom J. F., 2008, ApJ, 673, 999
Quimby R. M., Aldering G., Wheeler J. C., Höflich P., Akerlof C. W., Rykoff E. S., 2007, ApJ, 668, L99
Quimby R. M. et al., 2010, Astron. Telegram, 2979, 1
Quimby R. M. et al., 2011a, Nature, 474, 487
Quimby R. M. et al., 2011b, Astron. Telegram, 3465, 1
Racusin J. L. et al., 2009, ApJ, 698, 43
Rakavy G., Shaviv G., 1967, ApJ, 148, 803
Raskin C., Scannapieco E., Rhoads J., Della Valle M., 2008, ApJ, 689, 358
Rauw G., De Becker M., 2004, A&A, 421, 693
Rawlings S., Lacy M., Blundell K. M., Eales S. A., Bunker A. J., Garrington S. T., 1996, Nature, 383, 502
Resmi L. et al., 2012, MNRAS, 427, 288
Richardson D., Branch D., Casebeer D., Millard J., Thomas R. C., Baron E., 2002, AJ, 123, 745
Riess A. G. et al., 2007, ApJ, 659, 98
Sanders N. E. et al., 2012, ApJ, 758, 132
Sandoval M. A. et al., 2015, ApJ, 808, L32
Savaglio S., Glazebrook K., Le Borgne D., 2009, ApJ, 691, 182
Schlafly E. F., Finkbeiner D. P., 2011, ApJ, 737, 103
Schmidt B. et al., 2000, IAU Circ., 7516, 1
Schulze S. et al., 2014, A&A, 566, 102
Schulze S. et al., 2015, ApJ, 808, 73
Smartt S. J., 2009, ARA&A, 47, 63
Smith N. et al., 2007, ApJ, 666, 1116
Sollerman J. et al., 2007, A&A, 466, 839
Stanway E. R., Levan A. J., Tanvir N., Wiersema K., van der Horst A., Mundell C. G., Guidorzi C., 2015, MNRAS, 446, 3911
Starling R. L. C. et al., 2011, MNRAS, 411, 2792
Strolger L.-G. et al., 2002, AJ, 124, 2905
Strolger L.-G., Dahlen T., Riess A. G., 2010, ApJ, 713, 32
Svensson K. M., Levan A. J., Tanvir N. R., Fruchter A. S., Strolger L.-G., 2010, MNRAS, 405, 57
Tanvir N. R. et al., 2010, ApJ, 725, 625
Thöne C. C., de Ugarte Postigo A., García-Benito R., Leloudas G., Schulze S., Amorín R., 2015, MNRAS, 451, L65
Ugliano M., Janka H.-T., Marek A., Arcones A., 2012, ApJ, 757, 69
Vergani S. D. et al., 2011, A&A, 535, A127
Vreeswijk P. M. et al., 2014, ApJ, 797, 24
Weidner C., Kroupa P., Bonnell I. A. D., 2010, MNRAS, 401, 275
Woosley S. E., 1993, ApJ, 405, 273
Yusof N. et al., 2013, MNRAS, 433, 1114

Downloaded from http://mnras.oxfordjournals.org/ at California Institute of Technology on June 2, 2016

APPENDIX A

Table A1. SLSNe discovery images used for carrying out astrometry and identifying host galaxies. Details for images taken from literature can be found in the following sources [1]Rawlings et al. (1996), [2]ESO 59.A-9004(A), Service Mode, NTT, [3]Rezman Observatory, [4]GO-10877, PI: Li , [5]Barbary et al. (2009), [6]Gal-Yam et al. (2009), [7]Chatzopoulos et al. (2011), [8]ToO ESO, [9]Service Mode, NTT, [10]Discovery images courtesy of PTF, [11]ToO Gemini South, [12]ToO Gemini North.

SLSN	Ref. image	Instrument
SN1995av	[1]	WHT
SN1997cy	–	–
SN1999as	[2]	ESO NTT
SN1999bd	–	–
SN2000ei	–	–
SN2005ap	[3]	RezmanI
SN2006gy	[4]	*HST*
SN2006oz	–	–
SCP06F6	[5]	*HST*
SN2007bi	[6]	ESO FORS2 VLT
SN2008am	[7]	ROTSE Keck
SN2008es	[8]	
SN2008fz	[9]	ESO NTT
SN2009jh	[10]	PTF/P60
PTF09atu	[10]	PTF/P60
PTF09cnd	[10]	PTF/P60
SN2010gx	[11]	GMOS Gemini-S
PTF10hgi	–	–
PTF10vqv	–	–
CSS111230	–	–
PTF11dij	[10]	PTF/P60
PTF11dsf	[10]	PTF/P60
PTF11rks	[10]	PTF/P60
SN2012il	[12]	GMOS Gemini-N

Table A3. LGRB subsample from SNAPSHOT survey.

Event	Redshift	RA(J2000)	Dec.(J2000)
GRB050824	0.828	00:48:56.260	+22:36:33.20
GRB051016B	0.9364	08:48:27.860	+13:39:19.60
GRB060218	0.0331	03:21:39.650	+16:52:01.30
GRB060505	0.089	22:07:03.380	−27:48:52.90
GRB060602A	0.787	16:03:42.500	+66:36:02.60
GRB060614	0.125	21:23:32.190	−53:01:36.50
GRB060729	0.54	06:21:31.840	−62:22:12.10
GRB060912A	0.937	00:21:08.110	+20:58:19.20
GRB061007	1.2622	03:05:19.59	−50:30:02.3
GRB061110A	0.758	22:25:09.850	−02:15:31.00
GRB070318	0.840	03:13:56.760	−42:56:46.80
GRB070521	1.3500	16:10:38.62	+30:15:22.1
GRB071010A	0.98	19:12:14.624	−32:24:07.16
GRB071010B	0.947	10:02:09.240	+45:43:49.70
GRB071112C	0.823	02:36:50.910	+28:22:16.80
GRB071112	1.1400	18:26:25.26	+47:04:30.00
GRB080430	0.767	11:01:14.660	+51:41:07.80
GRB080520	1.5457	18:40:46.37	−54:59:30.6
GRB080707	1.2322	02:10:28.41	+33:06:34.5
GRB080805	1.5042	20:56:53.47	−62:26:40.2
GRB080916A	0.689	22:25:06.360	−57:01:22.90
GRB081007	0.5295	22:39:50.500	−40:08:49.80
GRB090424	0.544	12:38:05.090	+16:50:15.70
GRB090618	0.54	19:35:58.400	+78:21:25.20
GRB091127	0.49	02:26:19.910	−18:57:08.90
GRB091208B	1.063	01:57:34.090	+16:53:22.70

Table A2. CCSNe comparison sample selected from the GOODs survey, for which we carry out photometric measurements, with redshifts and positions included.

Event	Redshift	RA(J2000)	Dec.(J2000)	$m_{\rm nIR}$ (AB mag)	$M_{\rm nIR}$ (AB mag)	r_{80} (nIR) (kpc)
SN2006aj	0.03	03:21:39.670	+16:52:02.27	19.702 ± 0.002	−16.250 ± 0.002	1.1 ± 0.4
SN2002hs	0.39	03:32:18.590	−27:48:33.70	22.362 ± 0.009	−18.897 ± 0.009	1.1 ± 0.3
SN2002fv	0.70	03:32:19.220	−27:49:34.00	23.971 ± 0.016	−18.608 ± 0.016	0.56 ± 0.13
SN2002hq	0.67	03:32:29.940	−27:43:47.20	19.162 ± 0.001	−23.323 ± 0.001	1.4 ± 0.5
SN2002kb	0.58	03:32:42.441	−27:50:25.08	19.221 ± 0.0014	−22.9378 ± 0.0014	1.4 ± 0.5
SN2002fz	0.84	03:32:48.598	−27:54:17.14	20.385 ± 0.002	−22.600 ± 0.002	0.9 ± 0.3
SN2003ba	0.29	12:36:15.925	+62:12:37.38	18.8852 ± 0.0009	−21.7071 ± 0.0009	1.2 ± 0.4
SN2003bb	0.96	12:36:24.506	+62:08:34.84	19.3208 ± 0.0016	−23.9609 ± 0.0016	1.3 ± 0.4
SN2003ew	0.58	12:36:27.828	+62:11:24.71	20.817 ± 0.005	−21.346 ± 0.005	1.3 ± 0.4
SN2003dx	0.51	12:36:31.772	+62:08:48.25	22.223 ± 0.004	−19.648 ± 0.004	0.56 ± 0.15
SN2003er	0.63	12:36:32.270	+62:07:35.20	19.1932 ± 0.0006	−23.1551 ± 0.0006	0.9 ± 0.3
SN2003en	0.54	12:36:33.179	+62:13:47.34	21.91 ± 0.11	−20.09 ± 0.11	0.60 ± 0.16
SN2003bc	0.51	12:36:38.130	+62:09:52.88	20.807 ± 0.0018	−21.0661 ± 0.0018	0.8 ± 0.3
SN2003dz	0.48	12:36:39.967	+62:07:52.12	23.81 ± 0.03	−17.93 ± 0.03	0.63 ± 0.16
SN2003N	0.43	12:37:09.140	+62:11:01.20	22.809 ± 0.008	−18.677 ± 0.008	0.66 ± 0.18
SN2003ea	0.98	12:37:12.066	+62:12:38.04	22.870 ± 0.009	−20.457 ± 0.009	0.71 ± 0.18
SN2002kl	0.41	12:37:49.350	+62:14:05.71	22.2 ± 0.2	−19.20 ± 0.2	0.57 ± 0.15

Downloaded from http://mnras.oxfordjournals.org/ at California Institute of Technology on June 2, 2016

Table A4. Above: core-collapse SNe drawn the [1]GOODS sample and from [2]Sanders et al. (2012) and [3]Lennarz, Altmann & Wiebusch (2012). Below: LGRBs from Ghosts [4]Savaglio et al. (2009, and references therein), [5]Resmi et al. (2012), [6]Hjorth et al. (2012),[7]Sollerman et al. (2007), [8]Perley et al. (2013), [9]Levan et al. (2007), [10]Cool et al. (2007), [11]Tanvir et al. (2010), [12]Krühler et al. (2011), [13]McBreen et al. (2010), [14]Holland et al. (2010), [15]Vergani et al. (2011), [16]Starling et al. (2011), [17]Abazajian et al. (2009), [18]Pérez-Ramírez et al. (2013), [19]Elliott et al. (2013), [20]Levan et al. (2014b), [21]Schulze et al. (2014).

Event	Redshift	RA(J2000)	Dec.(J2000)	m_{UV} (AB mag)	M_{UV} (AB mag)	ref.
SN2002fz	0.841	03:32:48.598	−27:54:17.14	22.36 ± 0.01	−20.636 ± 0.01	3
SN2002hq	0.669	03:32:29.94	−27:43:47.2	22.455 ± 0.021	−20.074 ± 0.021	1
SN2002if	0.321	01:50:04.51	+00:00:26.4	20.54 ± 0.044	−20.38 ± 0.044	3
SN2002kb	0.58	03:32:42.441	−27:50:25.08	21.337 ± 0.007	−20.839 ± 0.007	3
SN2002ke	0.577	03:31:58.77	−27:45:00.7	22.883 ± 0.019	−19.316 ± 0.019	1
SN2002kl	0.41	12:37:49.350	+62:14:05.71	23.81 ± 0.01	−17.595 ± 0.01	3
SN2003ba	0.286	12:36:15.925	+62:12:37.38	21.533 ± 0.197	−19.062 ± 0.197	3
SN2003bb	0.954	12:36:24.506	+62:08:34.84	21.444 ± 0.007	−21.836 ± 0.007	3
SN2003bc	0.511	12:36:38.130	+62:09:52.88	22.645 ± 0.008	−19.281 ± 0.008	1
SN2003dx	0.46	12:36:31.772	+62:08:48.25	23.917 ± 0.343	−17.745 ± 0.343	3
SN2003ea	0.89	12:37:12.066	+62:12:38.04	24.13 ± nan	−19.016 ± nan	3
SN2003ew	0.66	12:36:27.828	+62:11:24.71	22.603 ± 0.193	−19.874 ± 0.193	3
HST04Geo	0.937	12:36:44.432	+62:10:53.19	24.438 ± 0.03	−18.842 ± 0.03	1
HST04Riv	0.606	03:32:32.407	−27:44:52.84	26.992 ± 0.175	−15.315 ± 0.175	1
HST05Bra	0.48	12:37:21.764	+62:12:25.67	23.649 ± 0.023	−18.156 ± 0.023	1
HST05Den	0.971	12:37:14.773	+62:10:32.61	25.949 ± 0.106	−17.408 ± 0.106	1
SN2005hm	0.035	21:39:00.65	−01:01:38.7	21.5 ± 0.22	−14.599 ± 0.22	2
SN2005nb	0.023	12:13:37.61	+16:07:16.2	15.966 ± 0.011	−19.215 ± 0.011	2
SN2006ip	0.030	23:48:31.68	−02:08:57.3	17.263 ± 0.022	−18.459 ± 0.022	2
SN2006ir	0.02	23:04:35.68	+07:36:21.5	17.347 ± 0.027	−17.491 ± 0.027	2
SN2006jo	0.076	01:23:14.72	−00:19:46.7	18.073 ± 0.028	−19.676 ± 0.028	2
SN2006nx	0.137	03:33:30.63	−00:40:38.2	21.119 ± 0.192	−18.285 ± 0.192	2
SN2006sg	0.44	02:08:13.041	−03:46:21.93	22.991 ± 0.259	−18.608 ± 0.259	2
SN2006tq	0.26	02:10:00.698	−04:06:00.91	22.855 ± 0.617	−17.576 ± 0.617	2
SN2007I	0.021	11:59:13.15	−01:36:18.9	19.11 ± 0.07	−15.827 ± 0.07	2
SN2007ea	0.04	15:53:46.27	−27:02:15.5	15.49 ± nan	−20.715 ± nan	2
SN2007ff	0.05	01:24:10.24	+09:00:40.5	17.322 ± 0.027	−19.563 ± 0.027	2
SN2007gl	0.03	03:11:33.21	−00:44:46.7	17.057 ± 0.026	−19.183 ± 0.026	2
SN2007hb	0.02	02:08:34.02	+29:14:14.3	15.617 ± 0.009	−19.283 ± 0.009	2
SN2007hn	0.03	21:02:46.85	−04:05:25.2	18.295 ± 0.036	−17.577 ± 0.036	2
SN2010ah	0.049	11:44:02.99	+55:41:27.6	20.15 ± 0.12	−16.544 ± 0.12	2
GRB970228	0.695	05:01:46.7	+11:46:53	25.1 ± 0.23	−18.2 ± 0.2	4
GRB970508	0.8350	06:53:49.2	+79:16:19	25.59 ± 0.15	−17.56 ± 0.15	4
GRB970828	0.9580	18:08:31.6	+59:18:51	25.28 ± 0.29	−18.1 ± 0.3	4
GRB980425	0.0085	19:35:03.2	−52:50:46	15.77 ± 0.03	−17.46 ± 0.03	4
GRB980703	0.9660	23:59:06.7	+08:35:07	22.57 ± 0.06	−20.86 ± 0.06	4
GRB990705	0.842	05:09:54.5	−72:07:53	22.79 ± 0.18	−20.42 ± 0.18	4
GRB990712	0.434	22:31:53.061	−73:24:28.58	23.15 ± 0.08	−18.46 ± 0.08	4
GRB991208	0.706	16:33:53.51	+46:27:21.5	24.51 ± 0.15	−18.15 ± 0.15	4
GRB000210	0.846	01:59:15.6	−40:39:33	24.18 ± 0.08	−18.89 ± 0.08	4
GRB010921	0.435	22:55:59.90	+40:55:52.9	22.6 ± 0.1	−19.4 ± 0.1	4
GRB011121	0.360	11:34:26.67	−76:01:41.6	24.1 ± 0.1	−18.7 ± 0.1	4
GRB020405	0.698	13:58:03.12	−31:22:22.2	22.6 ± 0.05	−20.14 ± 0.05	4
GRB020819B	0.41	23:27:19.475	+06:15:55.95	20.31 ± 0.02	−21.33 ± 0.02	4
GRB020903	0.25	22:48:42.34	−20:46:09.3	21.6 ± 0.09	−18.79 ± 0.09	4
GRB030329	0.168	10:44:50.030	+21:31:18.15	23.33 ± 0.09	−16.16 ± 0.09	4
GRB030528	0.782	17:04:00.3	−22:37:10	21.92 ± 0.18	−22.58 ± 0.18	4
GRB031203	0.1055	08:02:30.4	−39:51:00	18.23 ± 0.17	−24.70 ± 0.17	4
GRB040924	0.859	02:06:22.52	+16:08:48.8	24.31 ± 0.28	−18.9 ± 0.3	4
GRB050525	0.606	18:32:32.560	+26:20:22.34	≥24.0	≥ − 18.586	5
GRB050824	0.8278	00:48:56.100	+22:36:32.00	23.77 ± 0.14	−19.28 ± 0.14	6, 7
GRB050826	0.296	05:51:01.590	−02:38:35.40	21.37 ± 0.28	−21.34 ± 0.28	4
GRB060202	0.785	02:23:22.940	+38:23:03.70	23.29 ± 0.07	−19.72 ± 0.07	8
GRB060218	0.0335	03:21:39.670	+16:52:0	20.5 ± 0.13	−15.85 ± 0.13	4
GRB060912A	0.937	00:21:08.11	+20:58:18.9	22.72 ± 0.04	−20.63 ± 0.04	9
GRB070612	0.6710	08:05.4	+37:15	22.48 ± 0.17	−20.19 ± 0.17	10
GRB080319B	0.93	14:31:41.04	+36:18:09.2	26.95 ± 0.12	−16.29 ± 0.12	11

Downloaded from http://mnras.oxfordjournals.org/ at California Institute of Technology on June 2, 2016

Table A4 *– continued*

Event	Redshift	RA(J2000)	Dec.(J2000)	m_{UV} (AB mag)	M_{UV} (AB mag)	ref.
GRB081109	0.979	22:03:11.50	−54:42:40.5	22.69 ± 0.06	−20.69 ± 0.06	12
GRB090328	0.7354	06:02:39.69	−41:52:55.1	22.64 ± 0.13	−20.26 ± 0.13	13
GRB090417B	0.345	13:58:44.8	+47:00:55	23.24 ± 0.53	−17.8 ± 0.5	14
GRB091127	0.49	02:26:19.87	−18:57:08.6	24.14 ± 0.16	−17.79 ± 0.16	15
GRB100316D	0.0591	07:10:30.63	−56:15:19.7	18.73 ± 0.09	−18.97 ± 0.09	16
GRB100418	0.6239	17:05:26.96	+11:27:41.9	22.61 ± 0.16	−19.97 ± 0.16	17
GRB100621A	0.5420	21:01:13.12	−51:06:22.5	21.79 ± 0.06	−20.34 ± 0.06	12
GRB100816A	0.8049	23:26:57.56	+26:34:42.6	23.08 ± 0.15	−20.02 ± 0.15	18
GRB110918	0.984	02:10:09.39	−27:06:19.6	22.04 ± 0.05	−21.35 ± 0.05	19
GRB101225A	0.85	00:00:47.48	+44:36:01.0	26.75 ± 0.13	−16.60 ± 0.13	20
GRB111209A	0.67	00:57:22.700	−46:48:05.00	25.75 ± 0.14	−16.82 ± 0.14	20
GRB120422A	0.28	09:07:38.38	+14:01:07.5	24.65 ± 0.12	−15.88 ± 0.12	21
GRB130427A	0.35	11:32:32.63	+27:41:51.7	22.84 ± 0.08	−18.29 ± 0.08	20

This paper has been typeset from a TEX/LATEX file prepared by the author.

Downloaded from http://mnras.oxfordjournals.org/ at California Institute of Technology on June 2, 2016